REPORT DOCUMENTATION PAGE

Form Approved
OMB No. 0704-0188

1. REPORT DATE *(DD-MM-YYYY)*	2. REPORT TYPE	3. DATES COVERED *(From - To)*
29-07-2014	Journal Article	

4. TITLE AND SUBTITLE
Evaluation of the VIIRS Ocean Color Monitoring Performance in Coastal Regions

5a. CONTRACT NUMBER

5b. GRANT NUMBER

5c. PROGRAM ELEMENT NUMBER
0601153N

6. AUTHOR(S)
Soe Hlaing, Tristan Harmel, Alexander Gilerson, Robert Foster, Alan Weidemann, Robert Arnone, Menghua Wang and Samir Ahmed

5d. PROJECT NUMBER

5e. TASK NUMBER

5f. WORK UNIT NUMBER
73-4628-A2-5

7. PERFORMING ORGANIZATION NAME(S) AND ADDRESS(ES)
Naval Research Laboratory
Oceanography Division
Stennis Space Center, MS 39529-5004

8. PERFORMING ORGANIZATION REPORT NUMBER
NRL/JA/7330--13-1715

9. SPONSORING/MONITORING AGENCY NAME(S) AND ADDRESS(ES)
Office of Naval Research
One Liberty Center
875 North Randolph Street, Suite 1425
Arlington, VA 22203-1995

10. SPONSOR/MONITOR'S ACRONYM(S)
ONR

11. SPONSOR/MONITOR'S REPORT NUMBER(S)

12. DISTRIBUTION/AVAILABILITY STATEMENT
Approved for public release, distribution is unlimited.

13. SUPPLEMENTARY NOTES

14. ABSTRACT

Ocean color (OC) remote sensing has entered a new phase with the successful deployment of the Visible Infrared Imager Radiometer Suite (VIIRS) sensor aboard the Suomi National Polar-orbiting Partnership (SNPP) satellite. The representativeness and accuracy of the VIIRS geophysical products need to be assessed before a wide use of these data by the scientific community. As an integral part of the VIIRS sensor calibration and validation efforts, our group has been continuously monitoring the validity of the VIIRS's OC and atmospheric data stream through time-series in-situ data acquired at the observatory sites which are part of the AERONET-OC network. This paper addresses the preliminary evaluations of the VIIRS sensor's performance for retrieving OC data of typical coastal water environments, by carrying out time-series, as well as qualitative and quantitative match-up comparisons analysis between in-situ and satellite retrieved OC data. Initial time-series match-up comparisons carried out for a year period (January to December, 2012) show that VIIRS data exhibits strong temporal and statistical agreements with AERONET-OC data demonstrating a potential in enhanced coastal water monitoring from space. VIIRS data of two NASA-OBPG processing schemes which apply different vicarious calibration gains and NOAA-IDPS system are analyzed based on in-situ data of LISCO and WaveCIS AERONET-OC sites which are located in Long Island Sound and Gulf of Mexico respectively as well as OC retrievals of the Moderate Resolution Imaging Spectroradiometer (MODIS) sensor aboard the Aqua satellite. The underlying cause of the discrepancies observed in VIIRS retrieved normalized water-leaving radiances is also investigated. Finally, as the NASA-OBPG and NOAA-IDPS processing schemes for ocean color data of the VIIRS sensor continue to evolve, the results underline the necessity for monitoring and assessing the validity and consistency of VIIRS' ocean color products, especially for coastal waters.

15. SUBJECT TERMS
ocean color radiometry, coastal waters, satellite, VIIRS, MODIS, AERONET-OC, validation, water-leaving radiance, SeaPRISM, Angstrom coefficient, aerosol optical thickness, atmospheric correction

16. SECURITY CLASSIFICATION OF:			17. LIMITATION OF ABSTRACT	18. NUMBER OF PAGES	19a. NAME OF RESPONSIBLE PERSON
a. REPORT	b. ABSTRACT	c. THIS PAGE			Alan Weidemann
Unclassified	Unclassified	Unclassified	UU	17	19b. TELEPHONE NUMBER *(Include area code)* (228) 688-6232

Remote Sensing of Environment 139 (2013) 398–414

Contents lists available at ScienceDirect

Remote Sensing of Environment

journal homepage: www.elsevier.com/locate/rse

Evaluation of the VIIRS ocean color monitoring performance in coastal regions

Soe Hlaing [a], Tristan Harmel [b], Alexander Gilerson [a,*], Robert Foster [a], Alan Weidemann [c], Robert Arnone [d], Menghua Wang [e], Samir Ahmed [a]

[a] Optical Remote Sensing Laboratory, City College, New York, NY 10031, USA
[b] Laboratoire d'Océanographie de Villefranche, Université Pierre et Marie Curie, Centre National de la Recherche Scientifique, Villefranche-sur-Mer, France
[c] Naval Research Laboratory, Stennis Space Center, MS 39529, USA
[d] University of Southern Mississippi, MS 39529, USA
[e] NOAA/NESDIS Center for Satellite Applications and Research, College Park, MD 20740, USA

ARTICLE INFO

Article history:
Received 21 March 2013
Received in revised form 22 July 2013
Accepted 17 August 2013
Available online 17 September 2013

Keywords:
Ocean color radiometry
Coastal waters
Satellite
VIIRS
MODIS
AERONET-OC
SeaPRISM
Validation
Water-leaving radiance
Angstrom coefficient
Aerosol optical thickness
Atmospheric correction

ABSTRACT

Ocean color (OC) remote sensing has entered a new phase with the successful deployment of the Visible Infrared Imager Radiometer Suite (VIIRS) sensor aboard the Suomi National Polar-orbiting Partnership (SNPP) satellite. The representativeness and accuracy of the VIIRS geophysical products need to be assessed before a wide use of these data by the scientific community. As an integral part of the VIIRS sensor calibration and validation efforts, our group has been continuously monitoring the validity of the VIIRS's OC and atmospheric data stream through time-series in-situ data acquired at the observatory sites which are part of the AERONET-OC network. This paper addresses the preliminary evaluations of the VIIRS sensor's performance for retrieving OC data of typical coastal water environments, by carrying out time-series, as well as qualitative and quantitative match-up comparisons analysis between in-situ and satellite retrieved OC data. Initial time-series match-up comparisons carried out for a year period (January to December, 2012) show that VIIRS data exhibits strong temporal and statistical agreements with AERONET-OC data demonstrating a potential in enhanced coastal water monitoring from space. VIIRS data of two NASA-OBPG processing schemes which apply different vicarious calibration gains and NOAA-IDPS system are analyzed based on in-situ data of LISCO and WaveCIS AERONET-OC sites which are located in Long Island Sound and Gulf of Mexico respectively as well as OC retrievals of the Moderate Resolution Imaging Spectroradiometer (MODIS) sensor aboard the Aqua satellite. The underlying cause of the discrepancies observed in VIIRS retrieved normalized water-leaving radiances is also investigated. Finally, as the NASA-OBPG and NOAA-IDPS processing schemes for ocean color data of the VIIRS sensor continue to evolve, the results underline the necessity for monitoring and assessing the validity and consistency of VIIRS' ocean color products, especially for coastal waters.

1. Introduction

The Suomi National Polar-orbiting Partnership (SNPP) spacecraft was successfully launched on October 28, 2011 bearing several Earth observing instruments, including the Visible-Infrared Imager Radiometer Suite (VIIRS). This mission enables the scientific community to pursue the Earth observation effort initiated by, among others, the Advanced Very High Resolution Radiometer (AVHRR) and the Moderate Resolution Imaging Spectroradiometer (MODIS) to provide long time-series of accurate data required for global climate monitoring (Murphy et al., 2001). The VIIRS characteristics are especially well-suited for ocean color (OC) radiometry applications such as oceanic algal biomass or coastal waters monitoring. The recent National Research Council report (Committee on Assessing Requirements for Sustained Ocean Color Research, 2011) defined several requirements in order to ensure the sufficient data quality for OC scientific exploitation. Among them, calibration methods and algorithms have been developed based on lessons learned from the Sea-Viewing Wide Field-of-View Sensor (SeaWiFS), which was operational between 1997 and 2010, and the currently operational MODIS sensors. These products are being distributed as evaluation products for assessment by the SNPP Science Team and the research community. With a view to producing the standard suite of ocean color products from the VIIRS mission, it is now time to evaluate and validate the OC products estimated from the VIIRS measurements and to highlight their specific quality and sensitivity to the environmental conditions.

In processing of these evaluation products, NASA is deriving a continuous temporal calibration based on the on-board calibration measurements for the visible bands, and then reprocessing the full mission to produce a continuously calibrated sensor data records (SDR) product. The calibration of the NASA-VIIRS ocean color products is based on

* Corresponding author. Tel.: +1 212 650 8413.
E-mail address: gilerson@ccny.cuny.edu (A. Gilerson).

0034-4257/$ – see front matter © 2013 Elsevier Inc. All rights reserved.
http://dx.doi.org/10.1016/j.rse.2013.08.013

results from the prelaunch characterization (e.g., spectral response, polarization sensitivity, and response versus scan), and on-orbit temporal calibration (lunar measurements and solar diffuser measurements). In addition, the Ocean Biology Processing Group (OBPG) of NASA applies an additional vicarious calibration during SDR to OC Level-2 processing (Franz, Bailey, Werdell, & McClain, 2007; Gordon, 1998; Wang & Gordon, 2002; Werdell, Bailey, Franz, Morel, & McClain, 2007). In this latest processing (version 2012.2), the vicarious calibration is derived from the Marine Optical Buoy (MOBY) data (Clark et al., 1997, 2003). However, the MOBY mooring is located amid open ocean environment near Hawaii islands. Thus, evaluation of the VIIRS ocean color product is still necessary for coastal waters to assess the consistency of the overall calibration process. On the other hand, fulfilling the mission of the U.S. National Oceanic and Atmospheric Administration (NOAA), Interface Data Processing Segment (IDPS) developed by Raytheon Intelligence and Information Systems for the processing of the environmental data records (EDR) from SDR has gained beta status in January 2013 for evaluation. IDPS processing schemes for the VIIRS data differ from those of NASA in significant ways even at the SDR level. First, NOAA temporal calibration is changed at discrete intervals (currently daily, but less frequent in early mission) whereas NASA calibration is derived as a continuous trending from the start of the mission as mentioned above. Second, the NOAA calibration currently primarily uses the solar calibration (i.e., measurements from Solar Diffuser), while NASA OBPG uses both solar and lunar data. The procedure effectively supersedes the prelaunch absolute calibration. This step is applied as an effort to resolve absolute and spectral-relative calibration errors, which the NASA OBPG is currently resolving through a vicarious calibration that is applied in Level-2 processing. Thus, assessments are also necessary to evaluate the validity of the IDPS processing scheme.

The overall optical complexity of the atmospheric-water system makes observation of coastal waters from space highly challenging but of paramount importance for monitoring global water quality and assessing anthropogenic impacts (IOCCG, 2008). The ocean color component of the Aerosol Robotic Network (AERONET-OC) has been designed to support long-term satellite ocean color investigations through cross-site measurements collected by autonomous multispectral radiometer systems deployed above water (Hooker, Zibordi, Berthon, & Brown, 2004; Zibordi, Mélin, Hooker, D'Alimonte, & Holben, 2004; Zibordi, Mélin, et al., 2009). As part of this network, the Long Island Sound Coastal Observatory (LISCO) near New York City and WaveCIS in the Gulf of Mexico expand those observational capabilities with continuous monitoring as well as (for the LISCO site) additional assessment of the hyperspectral properties of coastal waters (Harmel et al., 2011).

In this study, the quality of the VIIRS products estimated through the OC processing, namely the normalized water-leaving radiances and atmospheric products (i.e., aerosol optical thickness and Angstrom exponent), are analyzed for typical coastal waters conditions encountered at LISCO and WaveCIS sites. Through statistical analysis carried out between the VIIRS, MODIS-Aqua and AERONET-OC data, the impacts of the different processing schemes (NASA's initial and latest version 2012.2, as well as IDPS) on the VIIRS's OC data retrievals are assessed. In particular, the impacts of the different processing procedures on the retrieved data quality are scrutinized in order to aid the scientific community to better interpret the physical or biogeochemical meanings of the VIIRS data in coastal areas. In the following section, the Background of the NASA ocean color satellite data processing is discussed along with the instruments and environmental characteristics of AERONET-OC sites used in this study. In Section 3, the spectral consistency of the VIIRS normalized water-leaving radiance retrievals of NASA OBPG processing schemes is firstly analyzed based on MODIS and in-situ SeaPRISM data. Then, the consistency, quality and uncertainty of those VIIRS data are also quantified through the time-series and match-up inter-comparison carried out with MODIS as well as SeaPRISM data. Processing algorithms employed in the IDPS system for OC data processing are firstly discussed in Section 4 and initial assessments of the IDPS VIIRS OC products are also made. In Section 5, the impacts of the retrieved atmospheric parameters on the estimation of the water-leaving radiance are discussed in order to delineate possible room for improvement in the overall VIIRS data processing. Summary and conclusions are presented in the last section.

2. Data and methods

2.1. Background of the NASA ocean color satellite data processing

In the ocean color satellite data processing, the atmospheric correction procedure, which eliminates the perturbing effects of the atmosphere and ocean surface, is the most important step. Notably the Near Infrared (*NIR*) algorithm developed by Gordon and Wang (1994a) which makes use of near infrared bands in initial estimations of water-leaving radiance, and the Short Wave Infrared (*SWIR*) algorithm that uses short wave infrared bands (Wang, 2007; Wang & Shi, 2005) and an approach which makes combined use of both *NIR* and *SWIR* algorithms (Wang & Shi, 2007) have been successfully used in the processing of ocean color (OC) data.

Total reflectance measured from the space-borne OC sensor at a wavelength (λ), denoted as $\rho_t(\lambda)$, can be described as following (Gordon & Wang, 1994a; IOCCG, 2010; Tanre, Herman, Deschamps, & Deleffe, 1979):

$$\rho_t(\lambda) = \rho_r(\lambda) + \rho_a(\lambda) + \rho_{ra}(\lambda) + T_s(\lambda)\rho_g(\lambda) + t(\lambda)\rho_f(\lambda) + t(\lambda)\rho_w(\lambda) \quad (1)$$

where ρ_r and ρ_a are the reflectances resulting from multiple scattering by air molecules (Rayleigh scattering) and aerosols, respectively. ρ_{ra} is the interaction term between molecular and aerosol scattering (Deschamps, Herman, & Tanre, 1983), ρ_f is the reflectance contribution from surface whitecaps and foam, ρ_g is the reflectance of the direct solar beam, and ρ_w is the water-leaving reflectance. T_s and t are the direct and diffuse atmospheric transmittance from surface to sensor direction respectively. In the current standard NASA processing, ρ_f is estimated according to Frouin, Schwindling, and Deschamps (1996) and Gordon and Wang (1994b). The ρ_g term is generally parameterized on the wind speed for a given viewing geometry (Wang & Bailey, 2001) using the Cox and Munk (1954) model. Similarly, ρ_r can be also well predicted from the atmospheric pressure and wind speed (Gordon & Wang, 1992; Hansen & Travis, 1974; Wang, 2002, 2005). The aerosol component ($\rho_a + \rho_{ra}$) is estimated through the *NIR* atmospheric correction algorithm (Gordon & Wang, 1994a), which is currently implemented with the set of aerosol models defined by Ahmad et al. (2010). In the standard NASA VIIRS processing, the *NIR* correction is applied iteratively in order to circumvent the difficulties associated with non-negligible water leaving radiance in *NIR* part of spectrum (Hu, Carder, & Muller-Karger, 2000; Ruddick, Ovidio, & Rijkeboer, 2000; Siegel, Wang, Maritorena, & Robinson, 2000; Stumpf, Arnone, Gould, Martinolich, & Ransibrahmanakul, 2003; Wang & Shi, 2005), the condition typically observed for turbid and highly productive coastal waters (Bailey, Franz, & Werdell, 2010; Siegel et al., 2000). In this approach, ρ_w is retrieved iteratively based on bio-optical models (Bailey et al., 2010; Bricaud, Morel, Babin, Allali, & Claustre, 1998; Sydor & Arnone, 1997). Finally, the standardized parameter, normalized water-leaving radiance $nLw(\lambda)$, is calculated as:

$$nLw(\lambda) = BRDF(\lambda)\frac{F_0(\lambda)}{\pi t_d(\lambda)}\rho_w(\lambda) \quad (2)$$

where *BRDF* is the correction factor for illumination and viewing geometries dependency which is the function of the constituents of water (Gordon, 2005; Hlaing et al., 2012; Morel, Antoine, & Gentili, 2002; Voss & Morel, 2005; Wang, 2006), F_0 is the extraterrestrial irradiance

(Thuillier et al., 2003) and t_d is the diffuse atmospheric transmittance along the Sun-to-surface direction.

2.2. Satellite data filtering procedures

The MODIS and VIIRS Level 2 images processed with the SeaDAS software package using standard iterative *NIR* atmospheric correction algorithm (Bailey et al., 2010; Gordon & Wang, 1994a; Siegel et al., 2000) have been obtained for the regions over the LISCO and WaveCIS sites for the January to December 2012 period from NASA OBPG website (http://oceancolor.gsfc.nasa.gov). For the VIIRS, data processed with initial as well as new processing (version 2012.2) schemes have been acquired. MODIS data used in this study is with MODIS-Aqua 2012.0 reprocessing. For the purpose of the abbreviation, VIIRS data processed with initial and version 2012.2 schemes will be from here on denoted as $VIIRS^{initial}$ and $VIIRS^{12.2}$, respectively. One of the major differences in those processing schemes is the vicarious calibration gains: [0.9627, 1.0008, 1.0092, 0.9747, 1.0147, 1.041 and 1.0] for the $VIIRS^{12.2}$ versus $VIIRS^{initial}$'s [0.9767, 1.0202, 1.0273, 0.9936, 1.0257, 1.047 and 1.0] for 410, 443, 486, 551, 671, 745 and 862 nm channels, respectively. In the initial processing ($VIIRS^{initial}$), the vicarious calibration reference was derived from a sea surface reflectance model and a climatology of chlorophyll-a concentration (Werdell et al., 2007). In the 2012.2 reprocessing ($VIIRS^{12.2}$), the vicarious calibration is based on measurements from the Marine Optical Buoy (MOBY) near Lanai Hawaii (the same reference is currently used for SeaWiFS and MODIS).

These standard Level 2 data files include the geophysical products of the atmospheric–ocean system, namely the aerosol optical thicknesses (τ_a), Angstrom coefficient (γ), the remote sensing reflectance (*Rrs*) which can be straightforwardly translated to normalized water-leaving radiance (*nLw*) by multiplying with F_0, and the level 2 quality flags. The VIIRS and MODIS data used in this study are with nadir resolutions of 750 m and 1 km, respectively. Those data have been processed for the sensor bands centered on following wavelengths: 410, 443, 486, 551, 671 and 862 nm for VIIRS and 412, 443, 488, 547, 667, and 869 nm for MODIS for the areas of two AERONET-OC sites, LISCO and WaveCIS. The pixels used for match-up comparison are all extracted from a smaller region (3 × 3 pixel box) centered at the site locations. In this study, we utilized the standard scheme, in which spatial average of satellite data from the region of interest is evaluated against temporally averaged in-situ data (Zibordi, Mélin, et al., 2009; Zibordi et al., 2004). In this approach, the data affected by the unexpected changes in the natural and environmental conditions as well as artifacts in the satellite image resulting from the sensor's intrinsic characteristics are excluded from the analysis using the filtering procedures which will be detailed in the next sections. Furthermore, any individual pixel is excluded from the match-up comparison process if it has been flagged, through the data processing, by at least one of these conditions: land, cloud, failure in atmospheric correction, stray light, bad navigation quality, both high and moderate glint, negative Rayleigh-corrected radiance, viewing angle larger than 60°, and solar zenith angle larger than 70°. Moreover, data of any individual pixels which have water-leaving radiance spectra with negative values in one of the wavelength are also excluded from spatial averaging. It should be noted here that all comparisons analysis will be carried out in reference to the SeaPRISM wavelengths (413, 442, 491, 551, 668 and 870 nm) from this point forward even though the satellite sensor wavelengths are slightly different from those of SeaPRISM for some channels.

2.3. In-situ AERONET-OC data

The ocean color component of the Aerosol Robotic Network (AERONET-OC) has been implemented to support long-term satellite ocean color investigations through consistent and accurate cross-site measurements collected by the SeaPRISM autonomous radiometer systems deployed on offshore fixed platforms. In addition to these ocean color measurements, the regular data acquisitions of AERONET are also carried out, which permit accurate retrievals of the aerosol optical thickness and the fine-coarse aerosol mode fraction. The SeaPRISM sea-viewing measurement sequence is executed every 30 min within plus or minus 4 h of 12:00 PM local time. The SeaPRISM data used in this study are level 1.5 data, and have been manually checked, making sure that no corrupted spectra were present in this dataset. The overall uncertainty of SeaPRISM *nLw* data has been estimated to be around ~5% for all wavelengths shorter than 668 nm for which uncertainty is about 7.8% (Zibordi, Mélin, et al., 2009). In this study, in-situ OC data retrieved at two specific AERONET-OC sites, namely LISCO and WaveCIS sites, are used to evaluate the VIIRS data.

The Long Island Sound Coastal Observatory (LISCO) platform combines a multispectral SeaPRISM system with a collocated hyper-spectral HyperSAS system (Satlantic, Canada) (Harmel et al., 2011) but data from the latter is not included in this analysis. The instruments are positioned on a retractable tower on the LISCO platform with an elevation of 12 m. They were installed in October 2009 and have been providing data since then. Recent recalibration of the LISCO SeaPRISM instrument at NASA showed only 0–1% deviations for all bands since a previous calibration in May 2011. The LISCO platform is located at approximately 3 km from the shore of Long Island near Northport, NY, USA. The coordinates of the site are N 40°57′16″, W 73°20′30″. Based on the time-series inherent optical properties (IOPs), which are derived from LISCO's one year SeaPRISM *nLw* data using the Quasi Analytic Algorithm (QAA) (Lee, Carder, & Arnone, 2002), particulate backscattering coefficient at 551 nm for LISCO water is observed to be in the range of 0.01 to 0.03 m^{-1}. Total absorption coefficient at 442 nm varies from 0.38 to 1.2 m^{-1}. The absorption due to Colored Dissolved Organic Matter (CDOM) at 442 nm is typically close to 0.4 m^{-1} and in few cases can be as high as 1 m^{-1}. The bathymetry in the vicinity of the platform exhibits a plateau at around 13 m depth and it has been verified that this depth is deep enough to make the sea bottom contribution to the water-leaving radiance negligible (Harmel et al., 2011).

The WaveCIS site is located at approximately 18 km from the shore of Timbalier Bay area, MS, USA. The coordinates of the site are N 28°52′ 00″, W 90°28′59″ and bathymetry in the vicinity of the platform is around 15 m. The SeaPRISM instrument is installed at 32 m height. Time-series IOPs of the WaveCIS water derived similar to the case of LISCO show that the particulate backscattering coefficient at 551 nm for WaveCIS water is usually around 0.01 m^{-1} but, in some rare cases, it is observed to be reaching up to 0.04 m^{-1}. Unlike LISCO water, total absorption of the water body is low with its seasonal average value equal to 0.31 m^{-1} at 442 nm of which ~0.15 m^{-1} is attributed to CDOM.

All in-situ data used in the quantitative match-up comparison analysis are selected from the measurements made within a ±2 h time window of the satellite overpass time of the locations of the sites. This approach ensures that the in-situ data set that is minimally affected by the natural temporal changes in the atmosphere and water and it is also in line with the similar validation exercises carried out for other OC sensors (Zibordi, Berthon, Mélin, D'Alimonte, & Kaitala, 2009; Zibordi, Mélin, et al., 2009; Zibordi et al., 2004). In addition, an in-situ data filtering criteria, which excludes the in-situ SeaPRISM data with high temporal variability from the analysis, was also applied to ensure the data used for the comparisons are not affected by the unexpected environmental changes. In this filtering procedure, we employ a particular statistical parameter, the relative standard deviation, which is denoted as σ_{rel} and calculated as $\sigma_{rel} = \sigma / \mu$ where σ and μ are the standard deviation and mean respectively of the data being considered for the match-up comparisons. In other words, σ_{rel} is the ratio of the standard deviation to the mean of the individual data points derived from the SeaPRISM measurements made within a ±2 h time window of the satellite overpass time, and is therefore a good indicator of the temporal variability within the data being considered. σ_{rel} is set to 0.2 for normalized water-leaving radiance match-up comparison analysis.

As for the time-series and qualitative comparison analysis, we only include the in-situ data derived from SeaPRISM measurements made between 16:15 and 19:30 GMT for LISCO site and between 17:20 and 20:00 GMT for WaveCIS respectively. These particular time periods of the day are selected so that the time ranges of in-situ data closely match the satellite overpass times for the sites which range from 17:15 to 18:27 GMT for LISCO site and 18:20 to 19:49 GMT for WaveCIS site. Finally, in-situ data derived from the measurements made while solar zenith angle is greater than 70° are also filtered out from all analysis.

3. Assessment of the NASA VIIRS normalized water-leaving radiance data

3.1. Analysis of the spectral consistency

Monitoring the seasonal and annual trends in the optical properties of ocean water primarily relies on the spectral characteristics of the retrieved $nLw(\lambda)$. A first step to evaluate the quality of the satellite retrievals is to determine whether they are spectrally representative of the actual optical properties of the water. The spectral consistency of the water-leaving radiances as retrieved by the VIIRS mission is examined based on the in-situ data collected over the VIIRS's entire operational period. Fig. 1 shows the $VIIRS^{initial}$, $VIIRS^{12.2}$, SeaPRISM and MODIS $nLw(\lambda)$ spectra recorded at the WaveCIS (1st row) and LISCO (2nd row) sites.

Notable is the larger number of satellite retrieved data available for the WaveCIS, than for LISCO. This is mostly due to the fact that there were fewer occurrences of atmospheric correction failures in satellite data retrievals for the WaveCIS site, which is located relatively further (13 km) from the shore than LISCO (~3.2 km). It should be noted here that, for LISCO site, after the application of quality flag conditions specified in satellite data filtering procedure, about 35% of the satellite retrieved $nLw(\lambda)$ spectra had to be further discarded from the analysis because of the presence of the negative values especially in violet (413 nm) and blue (442 nm) part of the spectrum. Conversely, for WaveCIS site, less than 5% are discarded for this reason. It was also observed that $VIIRS^{12.2}$ for LISCO site shows more frequent occurrences of the negative normalized water-leaving radiances especially at 413 nm wavelength resulting in less number of spectra available for match-up comparisons than $VIIRS^{initial}$. Out of the 40 $VIIRS^{12.2}$ matchups that pass quality flag conditions, 21 had to be further eliminated because of the negative values. The spectra in Fig. 3 further display the larger variability observable at the WaveCIS with respect to LISCO. Particularly, VIIRS spectra from WaveCIS exhibit values in the range of approximately 0.4–2.9 mW cm^{-2} μm^{-1} sr^{-1} at 551 nm, while spectra from LISCO are in the range of approximately 0.4–1.6 mW cm^{-2} μm^{-1} sr^{-1}. However, the comparison of match-up spectra and their averages and standard deviations indicates qualitative agreement between the satellites and SeaPRISM nLw data for both sites.

Additional insight from the qualitative analysis of VIIRS data and in-situ SeaPRISM data is presented in Figs. 2 and 3 for WaveCIS and LISCO sites, respectively. In these figures, the frequency distribution histograms

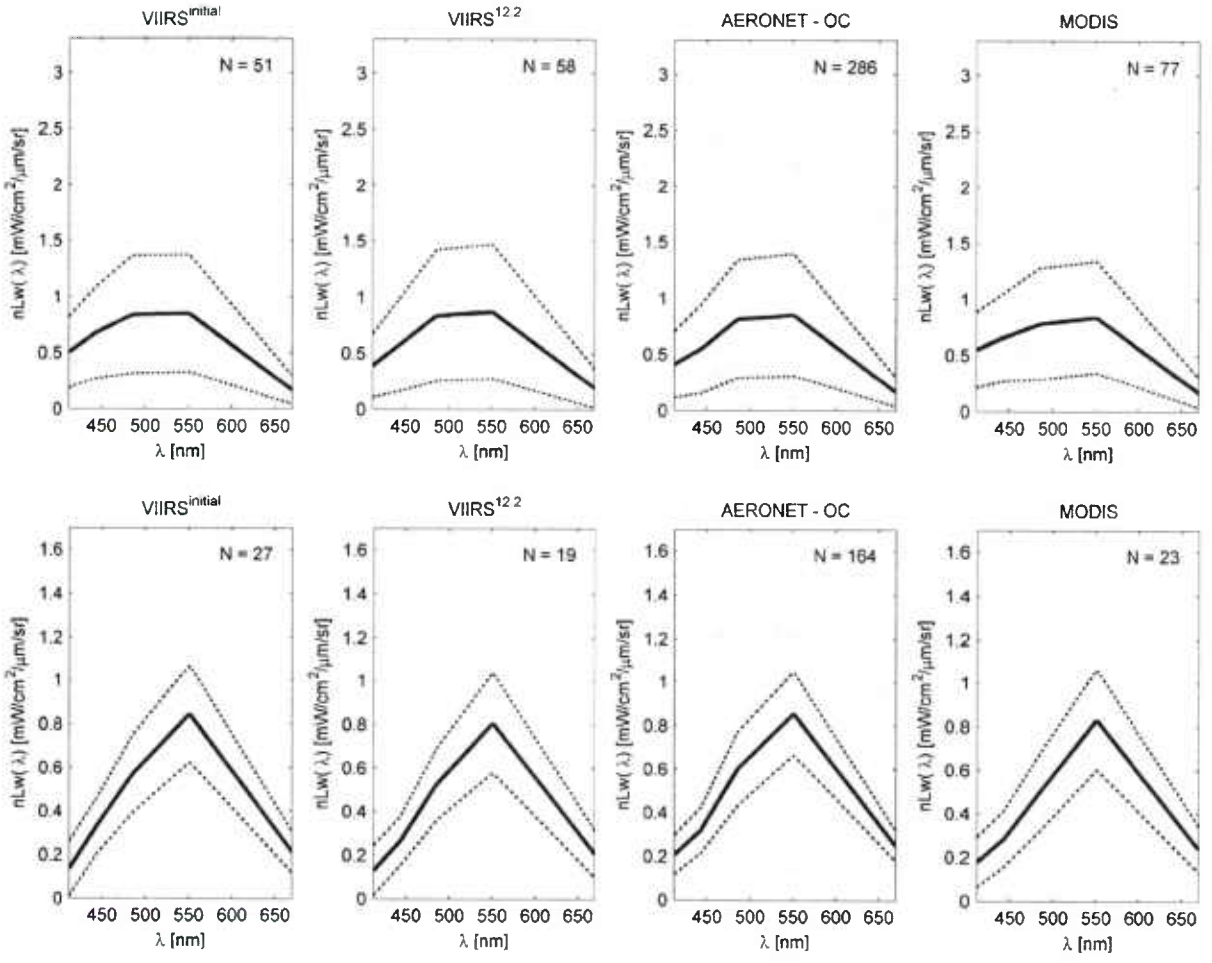

Fig. 1. $nLw(\lambda)$ match-up spectra of $VIIRS^{initial}$ (1st column), $VIIRS^{12.2}$ (2nd column), SeaPRISM (3rd column) and MODIS (4th column) for the WaveCIS (1st row)and LISCO (2nd row) sites. N is the total number of spectra for each sensor. Gray lines represent the individual spectra. Thick black solid lines indicate average and thick dashed lines indicate ±1 standard deviation.

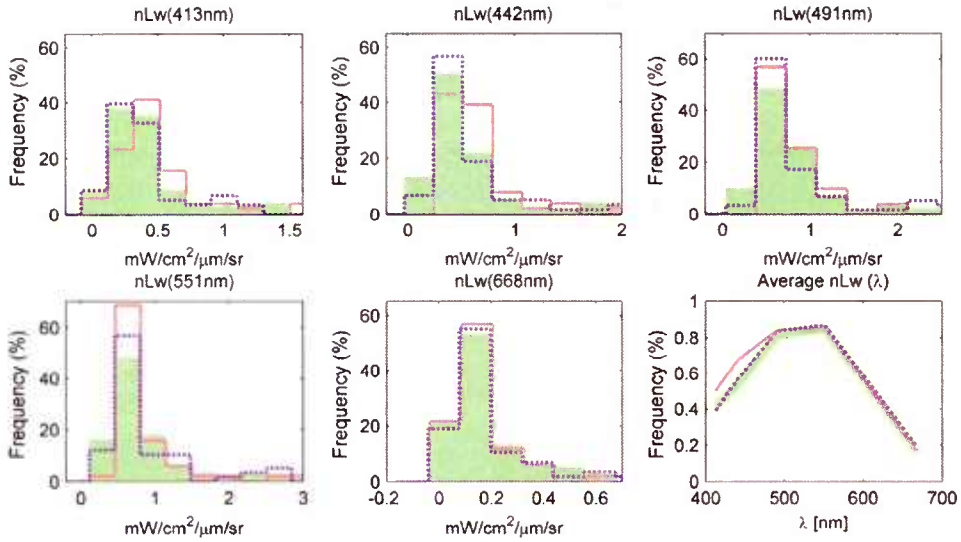

Fig. 2. Distributions of the *nLw* data at the WaveCIS site for VIIRS^{initial} (in brown), VIIRS$^{12.2}$ (in blue) and SeaPRISM (in green) at 413, 442, 491, 551, 668 nm along with the overall average *nLw*(λ) spectral (2nd row 3rd column).

of the *nLw*(λ) data of both VIIRS^{initial}, VIIRS$^{12.2}$ and SeaPRISM are displayed together for each individual spectral band. Thus, overall validity of the VIIRS data can be examined based on the matching of the *nLw* distributions for each wavelength. In addition, matchups of the overall average *nLw* spectra calculated from all available spectral data of the entire VIIRS operational period are also shown. For the WaveCIS site (see Fig. 2), it can be clearly observed that frequency distributions of the VIIRS$^{12.2}$ *nLw* data match better to those of SeaPRISM for every wavelengths than the VIIRS^{initial} demonstrating the advantages attained with the use of the new vicarious calibration gains for this site where contrasted water conditions are observed (i.e., clear to turbid waters). It can be also observed in the figure that the distributions of the *nLw* data at 413 and 442 nm for VIIRS^{initial} tend to skew to the right suggesting the overestimations in VIIRS data for those wavelengths compared to SeaPRISM. Cumulative effects of these overestimations in those wavelengths can be seen in the overall average *nLw*(λ) match-up comparisons (see Fig. 2 (last) for detail) (i.e. inconsistent spectral shape in the blue part of the spectra is observed for average VIIRS^{initial} *nLw* spectra).

On the other hand, for the LISCO site (see Fig. 3), distributions of the VIIRS *nLw* data of both processing are skewed to left compared to those of SeaPRISM at every wavelengths suggesting the overall underestimations in VIIRS retrieved data. Nevertheless, match-up comparisons exhibit that the average *nLw* spectra closely match to their counterparts in spectral shapes, values and ranges demonstrating the validity of the VIIRS retrieved data in a qualitative sense as well as the usefulness of the coastal AERONET-OC sites for the validation purpose. In terms of the spectral shape, VIIRS$^{12.2}$ exhibits the closest match to the SeaPRISM for WaveCIS site (see Fig. 2 (last)) but not for the LISCO turbid waters. The spectral shape inconsistencies of the both sites mostly appear at the shorter wavelength bands (412 and 443 nm) which are the most sensitive to atmospheric correction procedure.

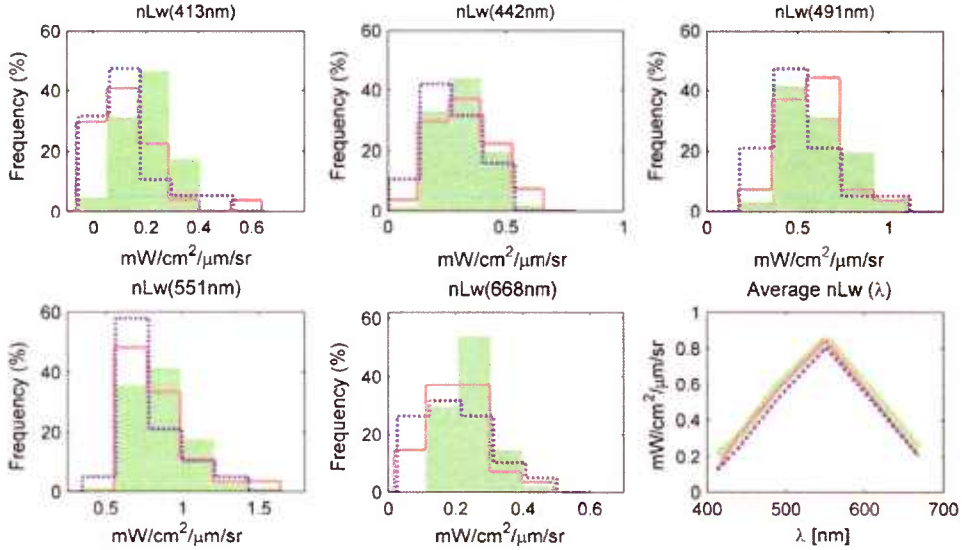

Fig. 3. Similar to Fig. 2 but for LISCO site.

3.2. Analysis of uncertainty in the VIIRS normalized water leaving radiance data

3.2.1. Comparisons of time-series data

Time-series of the VIIRS, MODIS and SeaPRISM $nLw(\lambda)$ data for the whole VIIRS operational period are displayed in Figs. 4 and 5 for WaveCIS and LISCO sites, respectively. For WaveCIS site time-series are shown for four SeaPRISM bands (413, 491, 551 and 668 nm) and, for LISCO site for three SeaPRISM bands (413, 551 and 668 nm). These bands are selected for the time-series analysis for the fact that the spectral characteristics of the $nLw(\lambda)$ data of the LISCO locations typically exhibit highest water-leaving radiance values at 551 nm whereas lowest values are always found at 413 and 668 nm wavelengths. On the other hand, for WaveCIS site, occurrences of highest water-leaving radiance values are not only frequently observed at 551 nm but also occasionally at 491 nm. Thus, assessment of the seasonal variations in the $nLw(\lambda)$ data can be effectively made through these bands.

3.2.2. Match-up comparison analysis between the satellite and in-situ data

The match-up comparison analyses between the observations which will be presented this point forward are based on linear regression between the any two data sets being compared. The comparisons are summarized through average percent differences, denoted as *PD*, and average absolute percent differences denoted as *APD* of *N* total number of matchups. The quantity *PD* determines the bias between the quantities being compared, while *APD* estimates the average uncertainty. The values of *PD* are calculated by averaging the percent differences between the matchups of the individual observations. Percentage difference of the *i*th matchup, PD_i is calculated by:

$$PD_i = 100\% \times \frac{y_i - x_i}{x_i}. \tag{3}$$

Similarly, *APD* values are calculated from APD_i calculated by following equation:

$$APD_i = 100\% \times \frac{|y_i - x_i|}{x_i} \tag{4}$$

where x_i and y_i stand for the any two data points being compared for the *i*th matchup and will be identified through the axis of the comparison figures of corresponding match-up analysis. In addition to these parameters, simple least square fit regression lines and coefficients of correlation (R) are computed at each wavelength for the comparisons in order to provide information on how well the data being compared match. Furthermore, match-up comparison filtering criteria which employs the so called two standard deviation filtering procedure (Zibordi et al., 2004) is also applied. In this procedure initial average (μ_{APD}) and standard deviation (σ_{APD}) of the all resulting APD_i between the two data being compared are firstly calculated. After that any matchups with the APD_i values greater than $\mu_{APD} + 2\sigma_{APD}$ are excluded from the match-up comparison analysis. This procedure is applied just to ensure that the values of the statistical parameters obtained from the match-up comparison analysis are not skewed by one or very few extreme cases whose statistics are entirely out of range of the majority of cases. It should be noted here that this procedure typically filter out only very few matchups (e.g., in the case of comparison between the VIIRS^{initial}

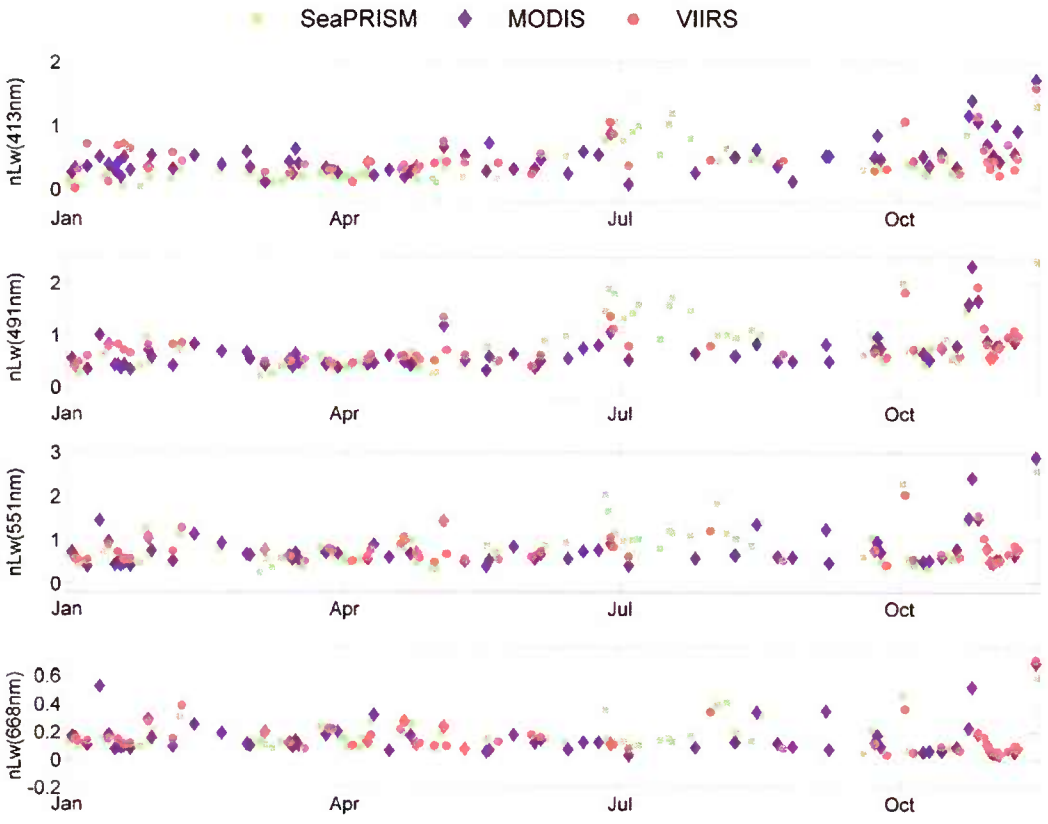

Fig. 4. Time-series of normalized water-leaving radiance, $nLw(\lambda)$ in mW/m^2/μm/sr, retrieved from SeaPRISM (green square), MODIS (purple diamond) and VIIRS (brown circle) at bands close to 413, 491, 551 and 668 nm for WaveCIS site.

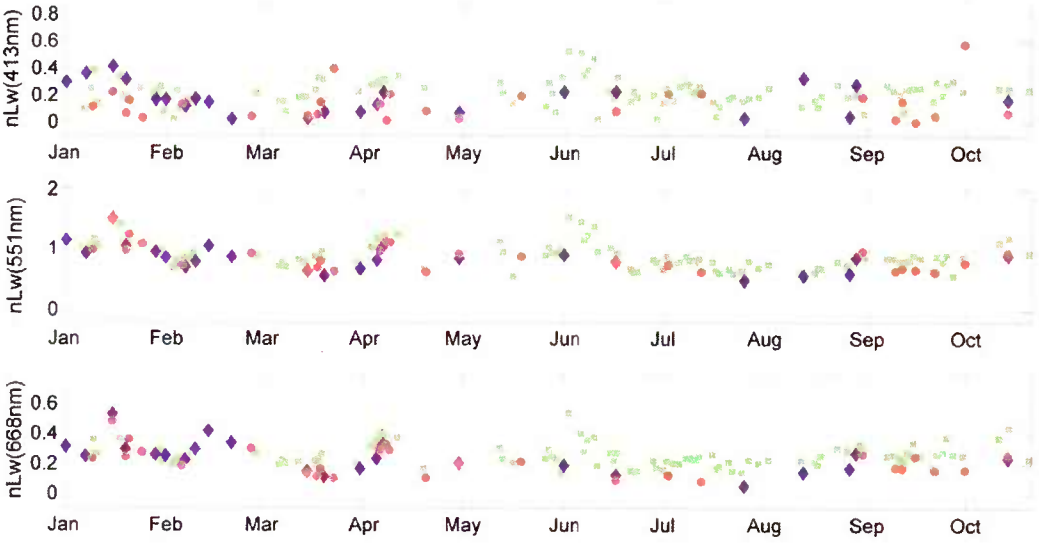

Fig. 5. The same as Fig. 4, but at the bands close to 413, 551 and 668 nm for LISCO site.

and SeaPRISM data for WaveCIS site, only 2 match-up points out of 143 are filtered out).

It has been observed that *nLw* data of the VIIRS$^{12.2}$ are lower than those of VIIRS^{initial} for both WaveCIS and LISCO sites. This observation is generally consistent with the vicarious calibration gain factors applied in the processing schemes (i.e., vicarious gains are lower in version 2012.2 processing scheme than the initial one) mentioned in Section 2.2. On spectral average, VIIRS$^{12.2}$ data is −16.35% and −18.17% lower than the VIIRS^{initial} for WaveCIS and LISCO site, respectively. It is also observed that resulting *PD* values between the VIIRS^{initial} and VIIRS$^{12.2}$ data at each wavelength for both sites show strong spectral dependencies exhibiting the tendency of displaying larger differences in the shorter end of the spectra. In addition, spectral shapes of *PD* values for two sites are also quite different from one to another. These observations point out that the impacts of the new processing scheme on sensor radiance data in retrieving *nLw* data is not the same for each site and are likely to be originated at least partially from the iterative nature of the atmospheric correction procedure for the *NIR* water-leaving radiances correction (Bailey et al., 2010). These may also arise from the procedures in computing the vicarious calibration gains. Vicarious calibration is generally performed using data from open ocean targets (in this case MOBY data) characterized by high spatial and temporal stability. These conditions ensure the generation of vicarious calibration coefficients mostly suitable for deep oligotrophic and mesotrophic waters, but validity of the use of these gains for the retrievals from coastal water areas should be further scrutinized (Zibordi, Berthon, et al., 2009).

3.2.2.1. Satellite and in-situ nLw match-up comparisons for WaveCIS site. The match-up comparisons of the satellite retrieved normalized water-leaving radiance $nLw(\lambda)$ data against in-situ SeaPRISM for WaveCIS are plotted in Fig. 6. Notable in the figures are the very high overall correlation coefficient (R) values (0.977, 0.974 and 0.961 for VIIRS$^{12.2}$, VIIRS^{initial} and MODIS respectively). Regression lines of all satellite to in-situ data comparisons are also very close to 1:1 line. Regression lines suggest that VIIRS$^{12.2}$ is slightly underestimated in terms of SeaPRISM data. Conversely, overestimation is observed in VIIRS^{initial}.

These observations confirm the results found in qualitative analysis where comparisons of average $nLw(\lambda)$ spectra showed the similar trend (see Fig. 4 for details). MODIS exhibits similar regression lines with that of VIIRS^{initial}, nevertheless few outliers exist at 413 and 442 nm wavelengths. These observations suggest the quantitative consistency between the all satellite and in-situ retrieved water-leaving radiance SeaPRISM data. Larger R values obtained for both VIIRS datasets compared with MODIS data may suggest the VIIRS's superior performance in retrieving water-leaving radiance data for WaveCIS location.

Overall percent difference *PD* values are −6.25, 13.8 and 19.16 for VIIRS$^{12.2}$, VIIRS^{initial} and MODIS comparisons, respectively. Therefore, it can be concluded that with the new processing scheme retrieval bias is reduced compared to initial one (see Tables 1 and 2 for details). R values obtained for comparisons between the *nLw* data of the SeaPRISM and satellite sensor at each wavelength range from 0.85 to 0.987 suggesting that variations in the water-leaving radiance data for WaveCIS location is well captured by all satellite sensors. This also points out the potential of both current and heritage OC sensors in better understanding of the inherent and apparent optical properties of the coastal waters through the improved data processing and correction procedures.

It is also observed that, with VIIRS^{initial}, *PD* values are equal to 23.2% and 32.3% for 413 nm and 442 nm wavelengths. However, with VIIRS$^{12.2}$, *PD* values for those wavelengths are equal to −13.8% and −6.2% suggesting the better spectral consistency in blue part of the spectra but with underestimations. This result again confirms the observations obtained in qualitative comparison analysis of previous section. For all other wavelengths greater than 442 nm, *PD* values range from −2.8% at 668 nm to −5.2% at 491 nm.

3.2.2.2. Satellite and in-situ nLw match-up comparisons for LISCO site. The match-up comparisons of the satellite retrieved normalized water-leaving radiance $nLw(\lambda)$ data against in-situ SeaPRISM for the LISCO site are shown in Fig. 7. A total of 81 SeaPRISM versus VIIRS^{initial}, 54 SeaPRISM versus VIIRS$^{12.2}$ and 49 SeaPRISM versus MODIS matchups are available for LISCO site. It is noticeable that fewer matchups between the satellite and in-situ SeaPRISM are available for LISCO site compared with WaveCIS site. As it has been shown in Fig. 3 of the qualitative analysis section above, retrieved *nLw* values at 413 nm wavelength for the LISCO location are typically in the range of 0.02 to 0.4 mW/cm^2/μm/sr with their average value equal to ~0.2 mW/cm^2/μm/sr whereas those of WaveCIS range between 0.05 and 1.5 mW/cm^2/μm/sr and the average value equal to 0.5 mW/cm^2/μm/sr. Thus, retrievals of water-leaving radiance especially at the blue part of the spectra for LISCO water type are much more sensitive to the atmospheric perturbation effects, and because of that, resulting in more frequent occurrences of negative values water-leaving radiance retrievals in the satellite data. Moreover,

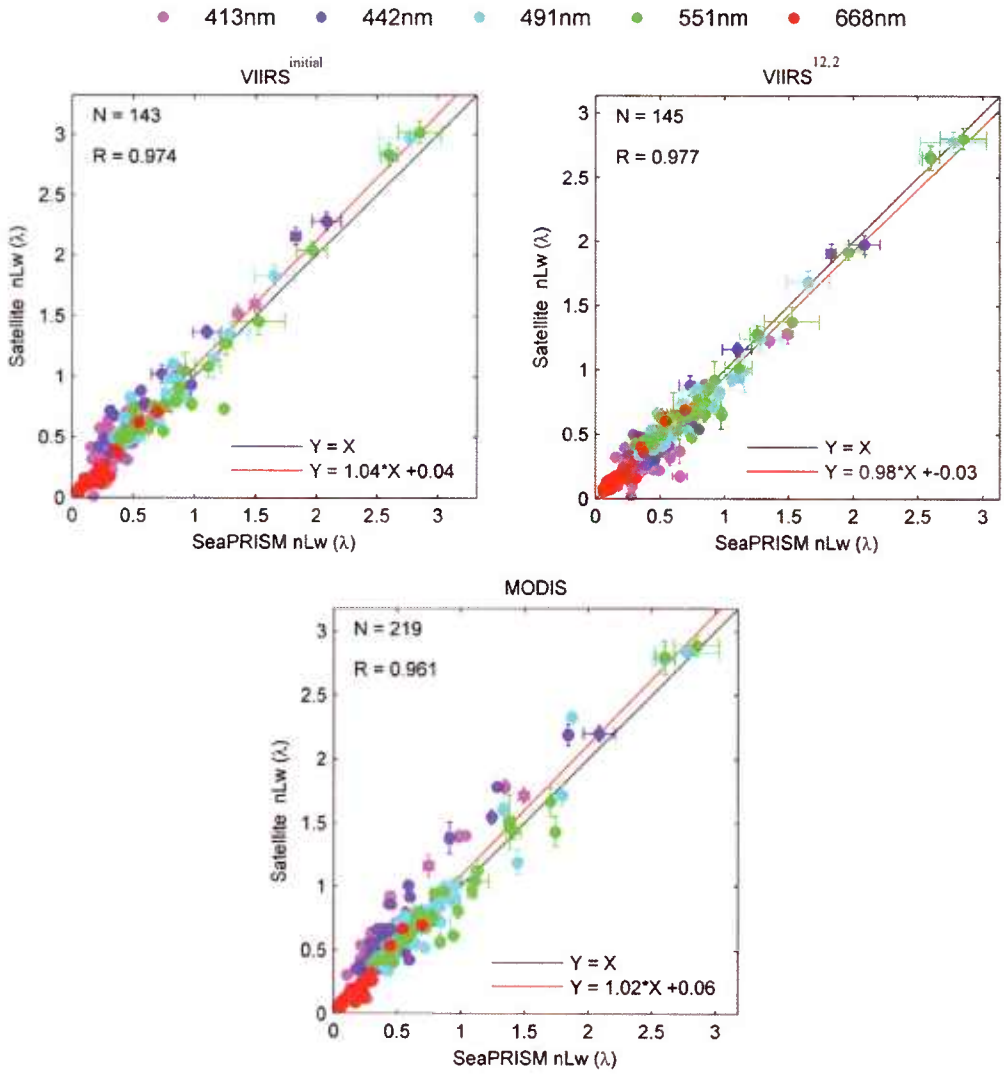

Fig. 6. Match-up comparison between the normalized water-leaving radiance $nLw(\lambda)$ (in mW/cm^2/μm/sr) retrieved from SeaPRISM and VIIRS^{initial} (1st row left), VIIRS$^{12.2}$ (1st row right) and MODIS (2nd row) for WaveCIS site. Horizontal and vertical error bars represent the temporal and spatial variations in SeaPRISM and satellite data, respectively.

it is observable that the number of matchups available is much less with MODIS than VIIRS^{initial}. Thorough investigations on the MODIS data reveals that more than 70% of the matchups with SeaPRISM are excluded by the application of stray light filter, the purpose of which is to eliminate the pixels that fall within very close proximity of very bright cloud and/or land pixels, after all other satellite data filtering procedures mentioned in Section 2.2 are applied. In contrast, with the VIIRS whose spatial resolution is higher than MODIS (750 m versus 1 km), only about half of the matchups are affected by this filter. This underscores the usefulness of the VIIRS's improved spatial resolution in ocean color remote sensing of coastal areas such as LISCO location for more data availability. It should be noted here that availability of very few matchups with the MODIS data for LISCO location force us to relax restrictions in the flag conditions applied in the data filtering procedures, and to include pixels that are flagged with moderate glint condition for the match-up comparison with the SeaPRISM. In overall, this step does not appear to affect the data quality of MODIS except for few observed outliers in blue part of the spectrum which are subsequently excluded from our analysis.

Similar to WaveCIS site, comparisons between the satellite and in-situ SeaPRISM data for LISCO achieve strong R values (0.961, 0.919 and 0.97 for VIIRS^{initial}, VIIRS$^{12.2}$ and MODIS respectively). It is observed that the VIIRS^{initial} data achieves the strong overall correlation with R value equal to 0.961. Moreover, the VIIRS^{initial} data also achieves strong correlations for the comparisons carried out at each individual wavelength: R values are equal to 0.8618, 0.9361 and 0.8276 at 491, 551 and 668 nm, respectively. However, at 442 nm only moderate correlation is attained with its R value equal to 0.5832. We believe that this observed degradation in the correlation between VIIRS and SeaPRISM data for 442 nm wavelengths is more likely to be originated from the data processing procedure rather than from the VIIRS sensor's characteristics. This conclusion is drawn based on the strong R value achieved at 668 nm wavelength of which nLw data range and distribution are similar to those of 442 nm. It should be also noted here that signal to noise ratio (SNR) of VIIRS sensor is higher at 442 nm (SNR $\approx$ 490) than at 668 nm (SNR $\approx$ 378).

Percent difference (PD) values obtained for the comparisons between the VIIRS^{initial} and SeaPRISM nLw data at all wavelengths suggest the underestimations in nLw retrievals in VIIRS^{initial}. Overall PD value is equal to 22.6% and underestimation is the highest at 412 nm wavelength with its PD value equal to -50%. But with the VIIRS$^{12.2}$, underestimations are further exacerbated to -26% on spectral average and overall uncertainty is further amplified. Degradations in correlation with in-situ data is also observed at every wavelength. At 442 nm

Table 1
Summary of statistical estimators for the comparisons between the VIIRS and SeaPRISM $nLw(\lambda)$ data of WaveCIS site. Results for $VIIRS^{initial}$ are shown in black and $VIIRS^{12.2}$ are in blue.

	Wavelengths (nm)					
Parameters	413	442	491	551	668	Overall
N	29 (29)	29 (29)	29 (29)	28 (29)	28 (29)	143 (145)
Regression	1.053x+0.05 0.83x–0.003	1.071x+0.103 0.97x–0.023	1.059x+0.025 1.01x–0.06	1.021x+0 0.98x–0.026	1.008x–0.01 0.99 x–0.007	1.04x–0.04 0.98x–0.03
R	0.917(0.862)	0.97 (0.963)	0.987 (0.987)	0.975 (0.986)	0.959 (0.962)	0.974 (0.977)
PD (%)	23.2 (–13.8)	32.3 (–6.3)	11.3 (–5.2)	4.7 (–3.1)	-2.5 (–2.9)	13.8 (–6.3)
APD (%)	41.5 (39.4)	33.2 (20.8)	13.9 (12.6)	12.5 (10.6)	16.1 (18.2)	23.4 (20.3)

correlation totally vanishes. More frequent occurrences of negative values retrieval in water-leaving radiance data are also observed resulting in less number of available match-up spectra. Thus, at the LISCO site, correlations for $VIIRS^{12.2}$ are noticeably lower than for $VIIRS^{initial}$ (see Table 3 for details). Summary of the statistical estimators for the comparisons between the MODIS and SeaPRISM nLw(λ) data of LISCO site can be found in Table 4.

In the match-up comparisons shown up to this point, it has been observed that the impact of the vicarious gain procedures on the retrievals of the *nLw* data are significant, although the changes in the gain values at each wavelength are relatively modest (i.e., ~1–2% except at the 862 nm channel whose gain is set to 1 for both processing schemes). It is due to the fact that the impacts of the these gain changes entirely fall on the water leaving (ρ_w) and aerosol ($\rho_a + \rho_{ra}$) components of the total radiance measurements (i.e., the estimation of the water-leaving reflectance (ρ_w), ρ_r, ρ_f and ρ_g terms in Eq. (1) are estimated from the parameters such as atmospheric pressure, wind speed and solar and sensor geometries). In the case of ($\rho_a + \rho_{ra}$) component, vicarious gain change in the 745 nm channel of VIIRS sensor will have direct impact on the determination of the aerosol model and concentration. Moreover, combined with the associated models, there may be further impacts in the estimation of the aerosol component in the visible bands during the iterative *NIR* correction process and in turn can have compounding impacts on the water leaving component. For the WaveCIS site of which water properties and atmospheric conditions are closer to those of open ocean conditions where vicarious calibration gains are derived from, spectral average retrieval biases are reduced down to −6.3% with $VIIRS^{12.2}$ from 13.8% with $VIIRS^{initial}$, in accordance with the new smaller vicarious gain values, compensating the positive retrieval bias in the initial processing scheme. On the other hand, for the LISCO site whose retrieved *nLw* values are already in underestimation, the use of the smaller gain values further exaggerated the underestimation to −26%, and, in addition, more occurrences of the negative water leaving radiances were observed. These observations outline the sensitiveness of the water leaving radiance retrieval process on the vicarious calibration procedures.

3.2.3. Match-up comparisons between the VIIRS and MODIS nLw data

In this section, VIIRS retrieved *nLw* data of both WaveCIS and LISCO locations are directly compared to those of MODIS. The main purpose of these comparisons is to analyze the consistency between the OC data retrieved from new VIIRS and heritage MODIS sensor, and from that to demonstrate whether the continuity of the reliable ocean color time-series data stream can be achieved. Here, all MODIS and VIIRS data used in the comparisons are filtered with the same quality flag conditions mentioned in Section 2.2. Match-up comparisons between the *nLw* data of VIIRS and MODIS for WaveCIS and LISCO locations are shown in Fig. 8. Overall consistency between the both VIIRS ($VIIRS^{12.2}$ and $VIIRS^{initial}$) and MODIS *nLw* data can be readily observed from the strong correlation coefficient (*R*) values obtained for the comparisons (*R* values equal to 0.972 and 0.984 with $VIIRS^{initial}$ for WaveCIS and LISCO sites respectively, and with $VIIRS^{12.2}$ they are equal to 0.954 and 0.982). However, for the comparisons between the $VIIRS^{12.2}$ and MODIS for both sites, regression lines significantly deviate from 1:1 line with the underestimations in $VIIRS^{12.2}$ retrieved *nLw* data in terms of the MODIS resulting in *PD* values of ~10% and ~26% for WaveCIS and LISCO sites, respectively. Underestimations in $VIIRS^{12.2}$ data are largest at the 413 nm with their *PD* values equal to −24% and −64% for WaveCIS and LISCO sites, respectively. However at 551 nm, *PD*s between $VIIRS^{12.2}$ and MODIS are lowest with their values equal to −5% and −7%, respectively, for WaveCIS and LISCO sites. On the other hand, for the comparisons between $VIIRS^{initial}$ and MODIS, regression lines are very close to 1:1 line for both sites. For LISCO site, *PD* values obtained for comparisons at individual wavelength are within ±2.6% except for the comparisons carried out at 413 nm and 491 nm wavelengths (whose *PD* values are equal to −31.5% and 7.4%, respectively). On the other hand, for WaveCIS site slight overestimations in $VIIRS^{initial}$ data are observed at every wavelength (*PD* values range from 4.7% at 413 nm to 11% at 668 nm).

Strong consistency in the time-series spectral *nLw* data retrieved from the two sensors can be observed particular through the large *R* values (0.745–0.994) obtained for the comparisons at every individual wavelength. For both $VIIRS^{12.2}$ and $VIIRS^{initial}$, correlation with the MODIS data tends to be strongest at 551 nm and weakest at 413 nm. For instance, *R* values obtained for the comparison between the $VIIRS^{initial}$ and MODIS data retrieved at the WaveCIS site are 0.8443 and 0.9938 at 413 and 551 nm wavelengths, respectively. Strong correlation at 551 nm can be mainly explained by the *nLw* spectral shapes that typically exhibit maximum water-leaving radiance at that wavelength for both WaveCIS and LISCO locations. Observed degradations in correlation at blue part of spectrum especially at 413 nm can be

Table 2
Summary of statistical estimators for the comparisons between the MODIS and SeaPRISM $nLw(\lambda)$ data of WaveCIS site.

	Wavelengths (nm)					
Parameters	413	442	491	551	668	Overall
N	43	45	44	43	44	219
Regression	1.2x + 0.084	1.11x + 0.103	1.048x − 0.007	0.976x + 0.034	1.02x − 0.003	1.02x + 0.06
R	0.936	0.956	0.976	0.967	0.963	0.962
PD (%)	48.3	35.4	4.2	4.2	3.6	19.2
APD (%)	52.8	38.0	12.9	11.2	17.5	26.5

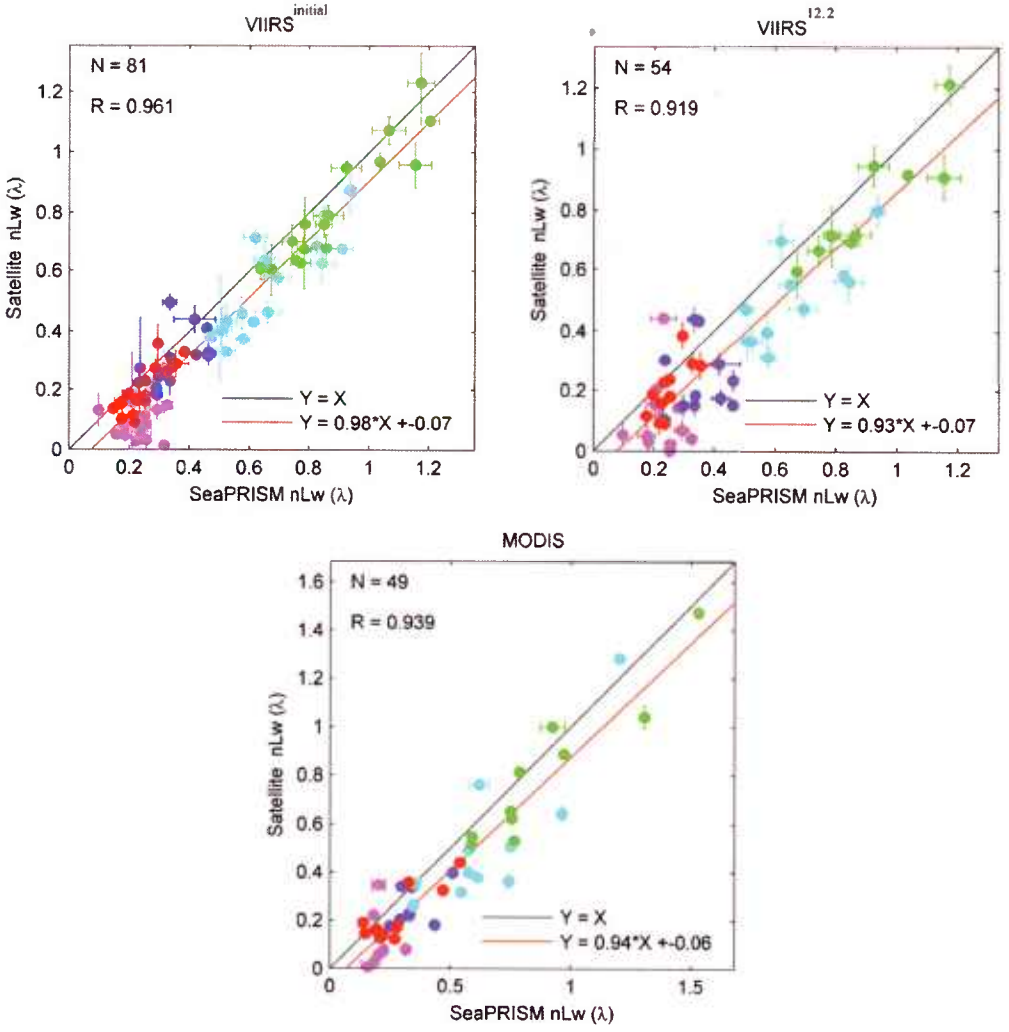

Fig. 7. Similar to Fig. 6, but for LISCO site.

mostly attributed to retrieval uncertainties resulted from the atmospheric correction procedures. Uncertainties between the *nLw* data retrieved by the two sensors are also highest at 413 nm with both VIIRS processing. At that wavelength, *APD* values obtained for the VIIRS versus MODIS *nLw* match-up comparisons at WaveCIS site are 43.63% and 44.2% for VIIRS$^{12.2}$ and VIIRS^{initial} data, respectively. For LISCO site, *APD* values at 413 nm are 64.29% and 50.3%. On the other hand, uncertainties between the *nLw* data retrieved from MODIS and VIIRS data are very low with *APD* equal to 3.9% at 551 nm for LISCO site with VIIRS^{initial} data. These observations combined with the strong correlation coefficients achieved at every wavelength for all comparisons carried out between the VIIRS and MODIS *nLw* data led us to conclude that variations in the water leaving radiance data are consistently well captured by both MODIS and VIIRS data but data processing procedures need to be improved for the consistent and accurate retrievals.

Here, it should be noted that all data involved in this analysis are processed using the same atmospheric correction procedures. Therefore it is reasonable to conclude that differences in the statistical parameter

Table 3
Summary of the statistical estimators the comparisons between the VIIRS^{initial} and in-situ SeaPRISM $nLw(\lambda)$data of LISCO site. Results for VIIRS^{initial} are shown in black and VIIRS$^{12.2}$are in blue.

	Wavelengths (nm)					
Parameters	413	442	491	551	668	Overall
N	16 (11)	16 (11)	17 (11)	16 (10)	16 (11)	81 (54)
Regression	−0.013x+0.11 −0.016x+0.11	0.626x+0.076 0.003x+0.236	0.924x−0.067 0.753x+0.011	1.032x−0.099 0.966x−0.058	1.012x−0.053 1.242x−0.109	0.98x−0.07 0.93x−0.07
R	−0.014 (0.0)	0.583 (0.002)	0.862 (0.743)	0.936 (0.893)	0.828 (0.732)	0.961 (0.919)
PD (%)	−50.6 (−49.3)	−14.7 (−29.8)	−18.3 (−23.0)	−8.4 (−10.1)	−21.2 (−20.9)	−22.6 (−26.6)
APD (%)	54.8 (66.0)	23.4 (45.0)	20.1 (25.3)	9.4 (11.3)	23.9 (26.4)	26.3 (34.8)

Table 4
Summary of statistical estimators for the comparisons between the MODIS and SeaPRISM $nLw(\lambda)$data of LISCO site.

	Wavelengths (nm)					
Parameters	413	442	491	551	668	Overall
N	9	8	11	10	11	49
Regression	0.504x − 0.012	0.5326x + 0.076	0.967 + 0.117	0.94x − 0.033	0.733x + 0.01	0.94x − 0.06
R	0.299	0.586	0.826	0.942	0.835	0.939
PD (%)	−31.2	−18.2	−21.6	−10.4	−20.8	−20.1
APD (%)	61.4	25.8	27.1	12.5	28.7	31.1

values obtained for the comparisons between the MODIS and two VIIRS data are almost entirely resulted from the different instrument calibration in producing SDR (or Level-1B data), as well as vicarious calibration factors applied to VIIRS sensor level data. On the other hand, for the previous re-processing of MODIS (R2010.0 and R2009.1), the MODIS-Aqua bands 8 and 9 (412 and 443 nm) were vicariously modified by the OBPG to adjust the temporal trends in the response versus scan angles (RVS). These temporal adjustments, which could not be fully characterized by the on-board (lunar, solar) calibration, were derived by cross-calibration with SeaWiFS (Meister, Franz, Kwiatkowska, & McClain, 2012). Similar to that, VIIRS to MODIS cross-calibration may be tested based on the observations made from the analysis carried out in this section for the consistent record of the ocean color data stream. It should be also noted that change of the processing scheme for the VIIRS sensor has different impact on the retrievals at two different coastal sites. These effects probably need to be considered before making decisions on changes of sensor gains.

4. Assessments of the IDPS VIIRS normalized water-leaving radiance data

In parallel with the NASA processing schemes, another data processing segment for sensor data of VIIRS is the ocean color component of the Interface Data Processing Segment (IDPS) developed by Raytheon Intelligence and Information Systems. IDPS provides all VIIRS operational data products including ocean color data. IDPS processes VIIRS along

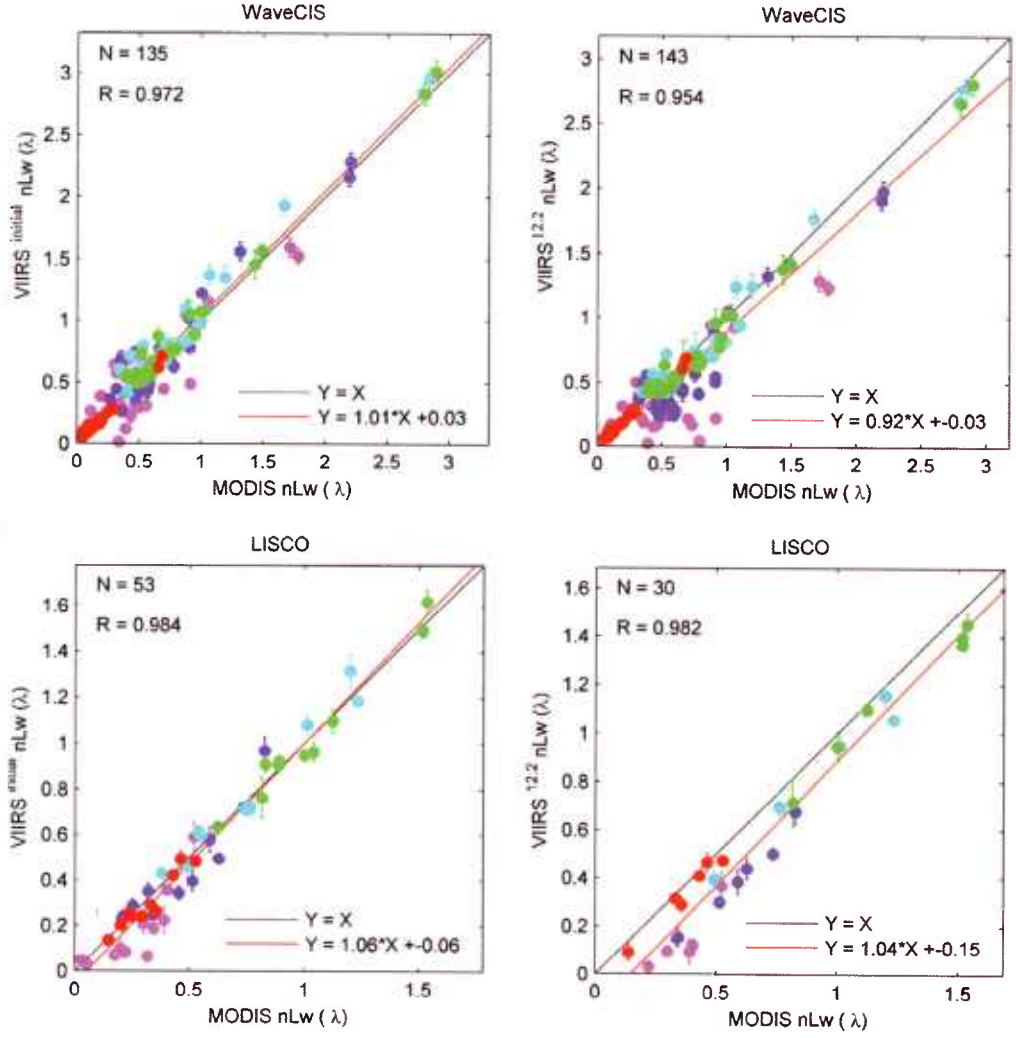

Fig. 8. Match-up comparison between the $nLw(\lambda)$ data of MODIS and VIIRS^{initial} (left), VIIRS$^{12.2}$ (right) for WaveCIS (1st row)and LISCO (2nd row) sites.

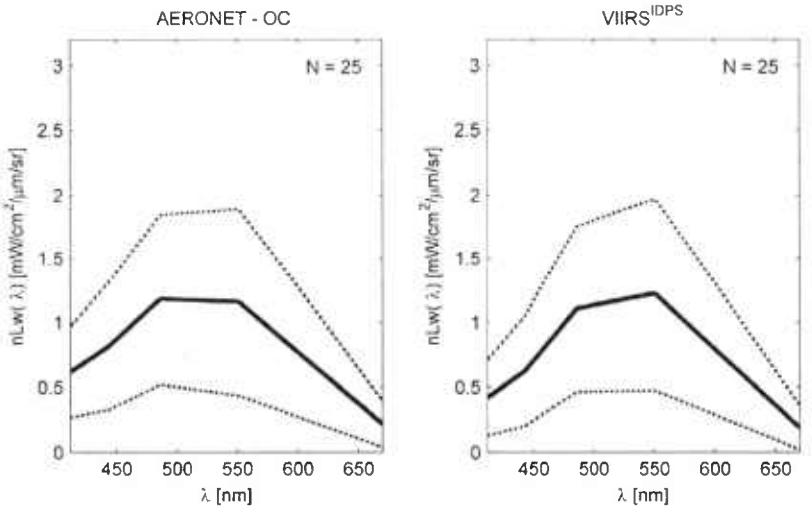

Fig. 9. $nLw(\lambda)$ match-up spectra of SeaPRISM (left), VIIRS^{IDPS} (right) for the WaveCIS site.

with other JPSS related sensor data to provide Environmental Data Records (EDR). IDPS system has been progressively developed taking into account the validation and calibration results to ensure the production of atmospheric and environmental products that meet strict accuracy and precision requirements, and it has gained beta status for evaluation. With the current operational IDPS OC EDR data has been produced since November 21, 2011, but pre February 6, 2012 data were assumed to be unreliable due to the calibration issues in the SDRs. In contrast to the NASA OBPG processing schemes, no vicarious calibration gain factors have been applied in the current operational IDPS OCC EDR processing. In the processing of OC EDR products in the IDPS framework, the *NIR* atmospheric correction procedure (Gordon & Wang, 1994a) is employed as in the NASA processing but with significantly different implementation. The main difference is in the aerosol models used for estimating the aerosol radiance component. In the IDPS, aerosol radiance contribution is estimated based on a family of 12 aerosol models (Gordon & Wang, 1994a; IOCCG, 2010) whereas NASA OBPG processing employs 80 aerosol modes (Ahmad et al., 2010). Of those 12 aerosol modes, the Oceanic, Maritime, and Tropospheric aerosol models are from Shettle and Fenn (1979), while the coastal aerosol model is introduced by Gordon and Wang (1994a). In particular, the IDPS OC data processing has not fully implemented yet for the *NIR* radiance correction (i.e., it assumes Black Ocean at the *NIR* bands for atmospheric correction, even over coastal turbid waters).

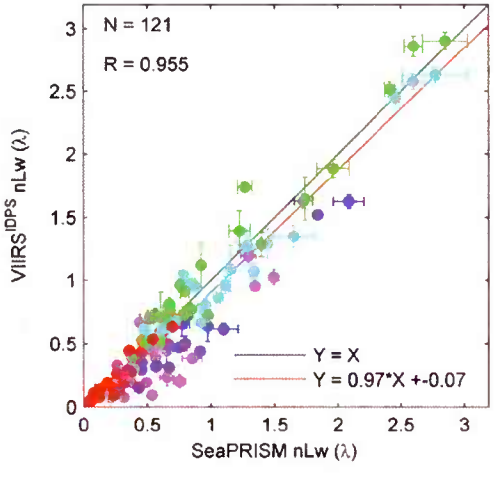

Fig. 10. Match-up comparison between the $nLw(\lambda)$ of SeaPRISM and VIIRS^{IDPS} for WaveCIS site.

As the processing system continue to evolve, we made initial assessments of the IDPS output of VIIRS *nLw* data in view of assisting the development of processing system for better retrieval of ocean color data especially in coastal zones. VIIRS Ocean Color/Chlorophyll EDR images processed with IDPS (version 6.6), from here on denoted as VIIRS^{IDPS}, of WaveCIS and LISCO location has been acquired from the NOAA's Comprehensive Large Array-Data Stewardship System (CLASS) website (http://www.class.ncdc.noaa.gov). Then, the *nLw* data of the locations of two sites are extracted in the same manner as for the NASA data. Similarly, the data used in the following analysis are filtered with the same quality control procedures described in Section 2.2. It should be noted here that, with IDPS processing, retrieved VIIRS *nLw* data points for match-up comparisons with SeaPRISM are more concentrated in the October–December period of 2012. For that reason, only the SeaPRISM data of the day for which VIIRS^{IDPS} is also available will be used for spectral consistency analysis, which is shown in Fig. 9. As the result, average spectral shape of the SeaPRISM data shown in Fig. 9 is slightly different from the one shown in Fig. 1 of Section 3 which is the seasonally averaged one. Fig. 9 shows the $nLw(\lambda)$ spectral of SeaPRISM (left) and VIIRS^{IDPS} (right) for WaveCIS that are coincidently retrieved within ± 2 h window and used for the match-up comparison analysis displayed in Fig. 10.

It can be observed in the figures that spectral variation ranges of the in-situ and satellite data are consistent to one another. Nevertheless, the overall average spectral shapes are notably different: average *nLw* spectrum of VIIRS^{IDPS} exhibits pronounces maxima at 551 nm. On the other hand, match-up comparison in Fig. 10 shows that VIIRS^{IDPS} data is strongly correlated with the in-situ SeaPRISM data exhibiting the overall *R* value of 0.955. In addition to that, correlations are also very strong at every wavelength (*R* values equal to 0.801 at 413 nm and 0.978 at 551 nm). VIIRS^{IDPS} underestimate at every wavelength but at 551 nm at which overestimation with *PD* value equals to 7.4%. For other wavelengths, underestimations range from −32% at 412 nm to −5% at 491 nm (see Table 5 for details). Overall, VIIRS^{IDPS} underestimates about 13% in terms of SeaPRISM on spectral average. On the other hand, for the LISCO site, out of 32 VIIRS^{IDPS} spectrums after filtered for the land, high sensor and solar zenith flag conditions, only 4 passed to the standard that is applied to all the satellite data throughout the paper. This is mostly due to issues related to the masking of the pixels with fill values for specific reasons (e.g., edge of swath and exclusion of coastal areas). These issues have been identified and are being progressively resolved by the ocean color EDR team. It should also be

Table 5
Summary of statistical estimators for the comparisons between the VIIRS^{IDPS} and SeaPRISM $nLw(\lambda)$ data of WaveCIS site.

	Wavelengths (nm)					
Parameters	413	442	491	551	668	Overall
N	25	24	24	24	24	121
Regression	0.674x − 0.001	0.819x − 0.056	0.94x − 0.002	1.008x − 0.051	0.908x − 0.009	0.908x − 0.009
R	0.801	0.923	0.975	0.978	0.946	0.955
PD (%)	−32.1	−26.0	−5.0	7.4	−11.3	−13.4
APD (%)	38.8	31.3	12.9	14.0	19.5	23.3

noted here that requirements for IDPS system do not specify the retrieval of ocean color data for coastal and in land waters. Fig. 11 shows the spectral match-up comparisons between the $nLw(\lambda)$ data of SeaPRISM and VIIRS^{IDPS} at the LISCO site for March 8th and 14th, June 10th and September 30th of 2012 for presentation purpose. It can be observed in the figures that the excellent agreement between the SeaPRISM and VIIRS^{IDPS} retrieved $nLw(\lambda)$ data for all comparisons except for June 10th. For that day, VIIRS^{IDPS} underestimates at all wavelengths but at 413 nm. It can be also observed that, for that day, the normalized water-leaving radiances at every wavelength are particularly high because of the strong particulate scattering resulted from the sediment discharge following a heavy rain event in New York region two days before. This led us to ponder this probably be due to incorrect negligible *NIR* water leaving radiance assumption made in the atmospheric correction of satellite data which in this case is clearly not correct. But for the definite conclusion, more observations and dedicated studies will be needed and beyond the scope of this paper. Although data availability is low for LISCO site, the observed consistencies between the SeaPRISM and VIIRS^{IDPS} data exhibits the potential of the IDPS system for the data retrievals of coastal areas.

The number of matchups at the LISCO site was not enough to make any conclusions but comparison of correlations and *PD* values for WaveCIS site estimated from matchups between VIIRS satellite and AERONET-OC data through NASA and IDPS processing schemes showed very similar results. At the same time the reasons for some observed spectral differences should be further investigated.

5. Evaluations on the retrieval performance of atmospheric parameters

5.1. Qualitative analysis of Angstrom coefficient distributions

As it has been shown in Section 2, the main step of the atmospheric correction procedure is to accurately estimate the $\rho_a + \rho_{ra}$ component. This is carried out based on the initial estimations of *NIR* aerosol radiance in conjunction with a suite of candidate aerosol models. Using the two most appropriate aerosol models with a weight, aerosol radiance at each desired wavelength is further derived (Gordon, Du, & Zhang, 1997; Wang, Knobelspiesse, & McClain, 2005). In this procedure, Angstrom exponent parameter, denoted as γ, is an estimator of the spectral behavior of the aerosol optical properties, and thus retrieval accuracy of γ is a good indicator of the quality of atmospheric correction process. Angstrom exponent (γ) is defined as (Wang et al., 2005):

$$\gamma = \frac{\log_e\left(\tau_a(\lambda_i)/\tau_a\left(\lambda_j\right)\right)}{\log_e\left(\lambda_j/\lambda_i\right)}. \quad (5)$$

Low values of the γ indicate the predominance of coarse aerosol; conversely, high values indicate a predominance of fine aerosols. It has been observed that the difference between NASA VIIRS aerosol optical thicknesses data obtained with the version 2012.2 and initial processing is less than 2.7% in 442 nm and 1.6% in 870 nm wavelengths. On the other hand, IDPS generates the pixel level atmospheric parameters only as intermediate products to be used in the generations of standard OC EDR products. These pixel level intermediate atmospheric products are not currently available for the evaluation. Therefore, for all analysis related to atmospheric parameters, we will use VIIRS$^{12.2}$ data only and refer simply as VIIRS in the comparisons. The histograms of the γ (442, 870) (i.e., Angstrom exponent defined between 442 and 870 nm) retrieved from satellite and AERONET measurements are shown in Fig. 12.

For the LISCO site (left), the histogram of the AERONET Angstrom exponent data (plotted in green) shows that the Angstrom exponent is almost always higher than 1 and can attain values as high as 3. This shows that the aerosols over LISCO site are typically dominated by fine aerosol particles. In contrast, the satellite Angstrom exponents for LISCO location are found to be always smaller than 2.2 and very frequently lie between 0 (spectrally flat aerosol) and 2. On average satellite

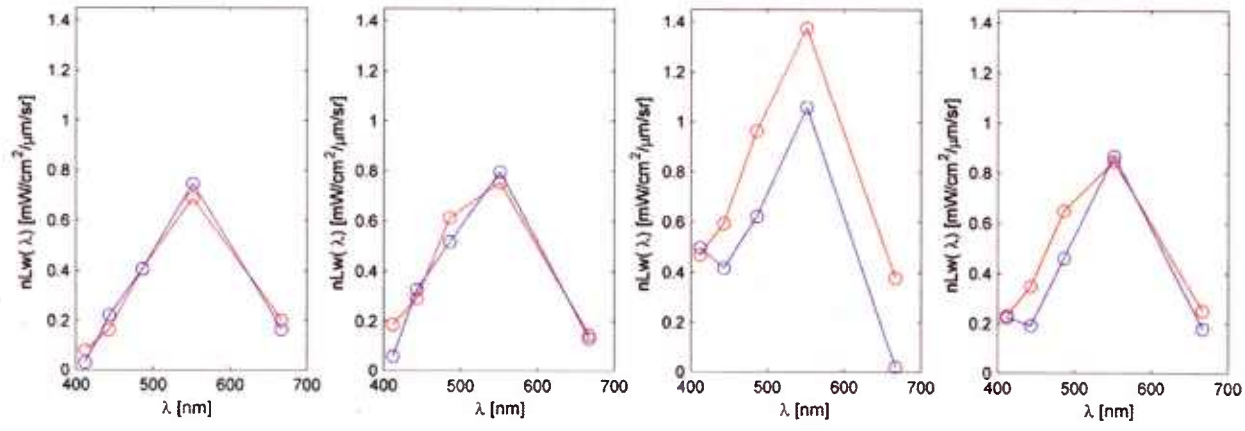

Fig. 11. $nLw(\lambda)$ spectral match-up comparisons of the SeaPRISM (plotted in red) and VIIRS^{IDPS} (blue) of the LISCO site for March 8th (1st column), March 14th (2nd column), June 10th and September 30th of 2012.

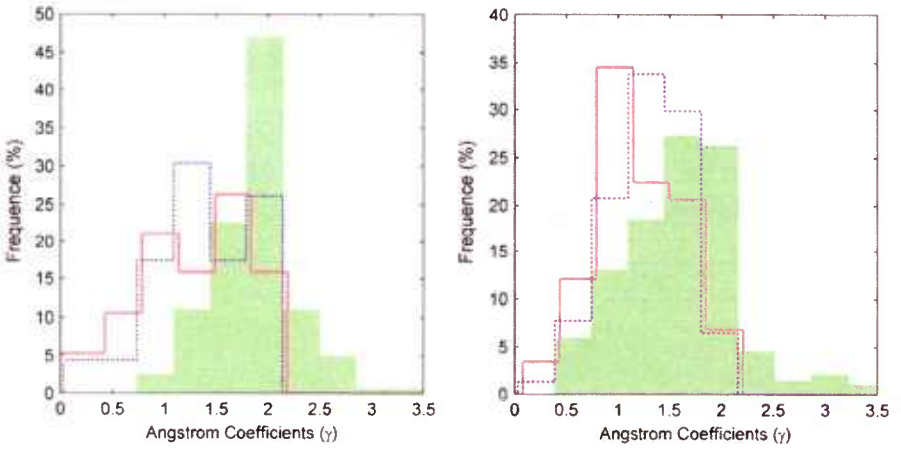

Fig. 12. Histograms of the % distribution of the Angstrom (γ) exponent values observed for the LISCO (left) and WaveCIS (right) sites. SeaPRISM is plotted in green, MODIS in blue dotted lines and VIIRS in brown thick lines.

retrieved γ values are about 0.66 lower than those retrieved from SeaPRISM. These results also confirm the findings of the similar study previously carried out by us with the use of the data from MODIS, MERIS and SeaWiFS (Ahmed et al., 2012).

It should be noted here that this observed discrepancy in the distributions of satellite and AERONET retrieved Angstrom exponent values are not limited to LISCO site alone. The same analysis carried out for the other AERONET sites: Brookhaven (located in Long Island) and

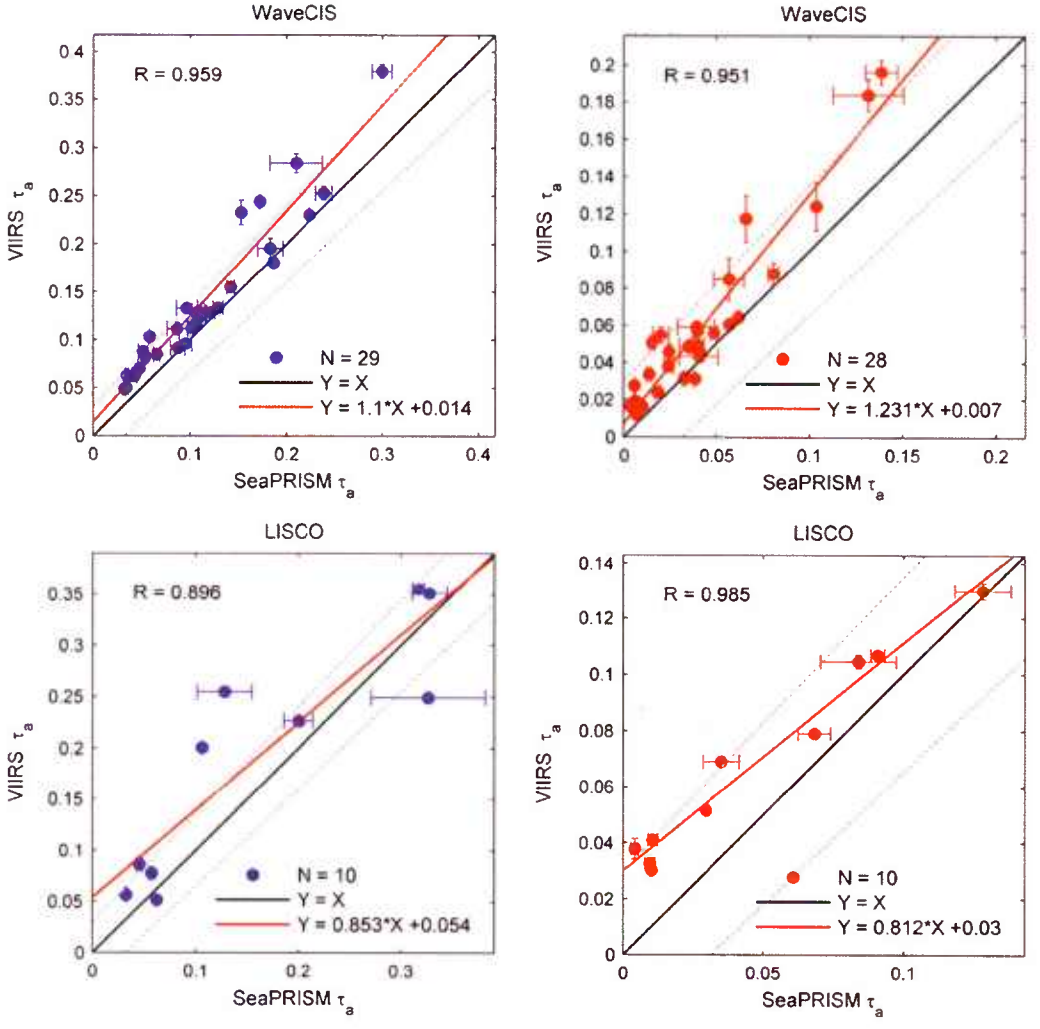

Fig. 13. Match-up comparisons of aerosol optical thickness τ_a at 443 nm (left) and 870 nm (right) derived from VIIRS and SeaPRISM measurements for WaveCIS site (1st row) and LISCO (2nd row). The red line is the regression line whose y is the equation and the dotted gray lines are the uncertainty level of the AERONET data.

COVE (in Chesapeake Bay), showed similar trend as at LISCO (not shown in this paper). Similarly for the WaveCIS site (right figure), the histogram of the AERONET γ data ranges from 0.4 to 3.5 whereas that of VIIRS and MODIS are in the range of 0.4 to 2.2. The distributions of satellite and AERONET Angstrom data match better than at LISCO but with underestimation of ~0.34 in satellite retrieved Angstrom values on average. These observations suggest that spectral behavior of the aerosol optical properties are relatively better captured at WaveCIS location. Strict upper bound of the satellite retrieval observed at LISCO location probably is resulted from the limited set of aerosol models used in the atmospheric correction procedure (Ahmad et al., 2010). On the other hand, it is also possible that it is at least partially resulted from the iterative procedures in the atmospheric correction process in the estimation of the aerosol components in the atmospheric radiance of *NIR* region (Bailey et al., 2010; Stumpf et al., 2003; Wang & Shi, 2005). Nevertheless, investigations on these observations of mismatch in the aerosol radiance spectral shape will require the detail analysis on the whole atmospheric correction procedures and are beyond the scope of this study.

5.2. Match-up comparisons of aerosol optical thickness data

The results of the match-up comparisons between VIIRS and SeaPRISM τ_a data taken around 443 and 870 nm are shown in Fig. 13. Both satellite and in-situ τ_a shown here correspond to normalized water-leaving radiance data of VIIRS and SeaPRISM presented in previous section. Similarly, *PD* and *APD* values for τ_a comparisons are calculated from data points that pass the satellite and in-situ water leaving radiance data filtering procedures mentioned in Section 2 to reflect the typical uncertainty encountered in retrieving water leaving radiance and atmospheric data. For both LISCO and WaveCIS sites, in-situ and satellite retrieved τ_a values are significantly correlated with values of the coefficient *R* equal to 0.959 and 0.951 at 443 and 870 nm wavelengths respectively for WaveCIS site, and 0.894 and 0.903 for LISCO site. These strong correlations at both 442 and 870 nm wavelengths suggest that VIIRS well captures the variations in the atmospheric changes at the location of the sites. On the other hand, overestimations in VIIRS retrieved τ_a values are observed for both sites at both 442 and 870 nm wavelengths. For WaveCIS site, *PD* values are 28% and 105% respectively for comparisons carried out at 442 and 870 nm, respectively. Similarly, observed *PD* values for LISCO are 38% and 108% respectively. Relatively higher *PD* values observed at 442 nm for LISCO site might be at least partially explained by the mismatch between the γ distributions of VIIRS and satellite data which in turn suggest possible inadequate aerosol mode selection for VIIRS. Although the observed discrepancies between the satellite and in-situ retrievals of aerosol optical thickness are high, these observations are not limited to LISCO and WaveCIS locations. Validation study carried out for MODIS data based on the data of other coastal AERONET-OC sites (AAOT, GLT and HLT) had also displayed such discrepancy (Zibordi, Berthon, et al., 2009). Interestingly, linear regression calculated for the comparisons between the τ_a data of SeaPRISM and

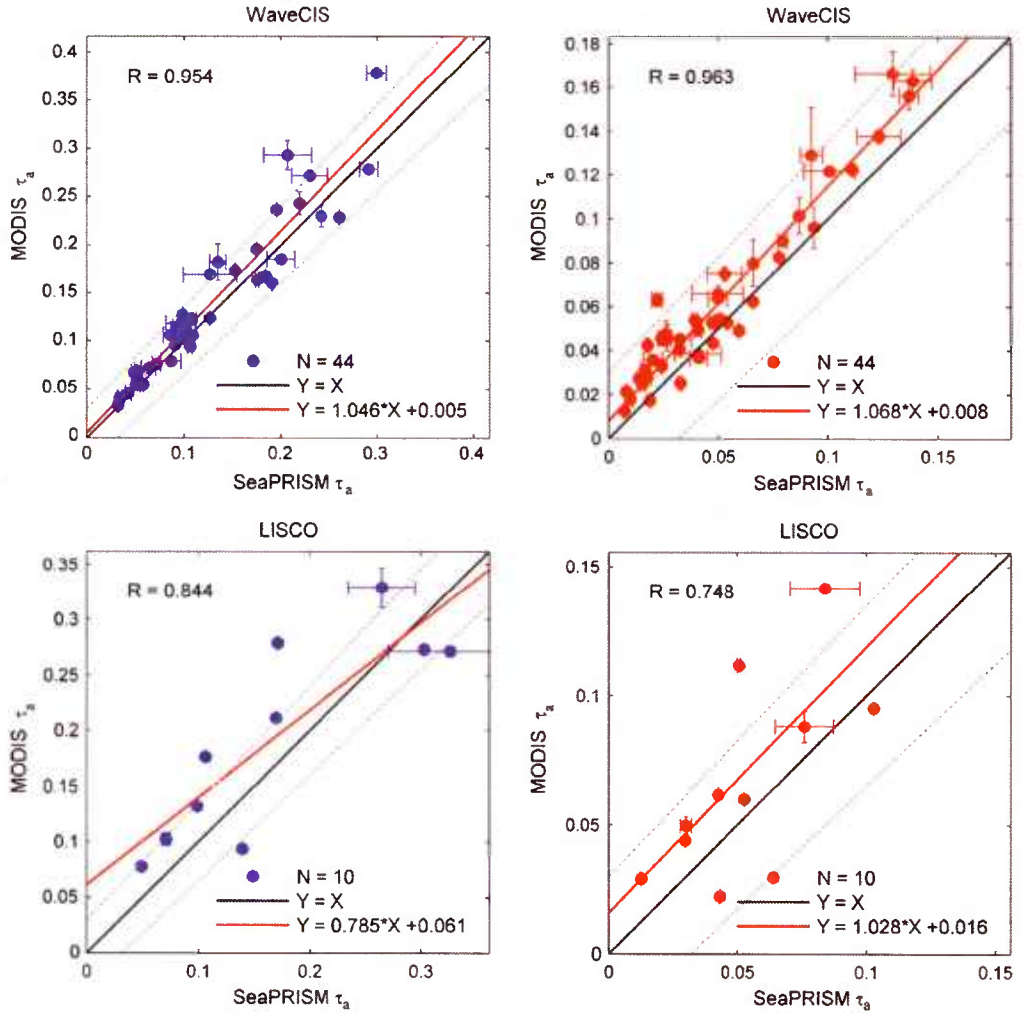

Fig. 14. Similar to Fig. 13 but for MODIS.

VIIRS at both wavelengths for both sites are close to the upper uncertainty level line of the SeaPRISM aerosol retrieval which is defined as $\tau_a \pm 0.05 \times \tau_a \pm 0.03$. The observed large overestimate of satellite derived τ_a likely results from uncertainties in the absolute radiometric calibration of the space sensor in the *NIR* (Bulgarelli & Zibordi, 2003), and additionally probably from the use of an inappropriate aerosol model.

In the following, we will further investigate the possible causes of observed discrepancies in τ_a retrievals with the use of MODIS data.

Similar to Fig. 13, the scatter plots in Fig. 14 show the comparisons of MODIS and SeaPRISM derived τ_a data. The regression lines of the comparisons suggest MODIS retrieved τ_a values are also overestimated for WaveCIS and LISCO sites as in the case of VIIRS. Nevertheless, overestimations in MODIS retrieved τ_a values are much less than those observed for VIIRS. *PD* values are 9% and 37% at 442 and 870 nm for WaveCIS site and 25% and 44% for LISCO site, respectively,.

Here, larger *PD* values observed at LISCO can be partially attributed to more pronounced mismatch in distributions γ values between the MODIS and SeaPRISM. We have been addressing the effect of the inappropriate aerosol mode selection on τ_a retrievals. However, this effect alone cannot entirely explain the overestimations with average *PD* value 108% at 870 nm observed for VIIRS data. On the other hand, overestimations in MODIS retrieved τ_a values are much lower (*PD* values are 37% and 44% at 870 for WaveCIS and LISCO respectively). It should be noted here that both VIIRS and MODIS data are processed with the same processing procedure. In addition, γ distributions observed for these two sensors closely match to each other for both sites (see Fig. 10). Therefore these significantly larger *PD* values observed for comparisons between VIIRS and in-situ SeaPRISM τ_a are probably originated from the uncertainties in the absolute radiometric calibration of the space sensor in 862 nm band of VIIRS. In fact, it is recalled that VIIRS data at the 862 nm center wavelength are not vicariously calibrated for both initial and new processing whereas the vicarious calibration of all visible channels is based on measurements from MOBY near Lanai Hawaii (the same reference currently used for MODIS). On the other hand, VIIRS's center wavelength (862 nm) is further from the center wavelength of SeaPRISM than MODIS's 869 nm. This might also in part contribute to the observed more pronounced discrepancies in VIIRS data.

6. Summary and conclusions

In the investigations carried out for over almost a year period dataset of VIIRS based on the data from two coastal AERONET-OC (LISCO and WaveCIS) sites, it has been observed that VIIRS sensor can well capture the seasonal and temporal variations in water properties. For both sites, in-situ and satellite retrieved *nLw* data are significantly correlated with values of the overall coefficient of correlation *R* equal to 0.968 for LISCO and 0.977 for WaveCIS, respectively. For the WaveCIS site, it was observed that VIIRS$^{12.2}$ *nLw* data match better to those of SeaPRISM for every wavelength than the VIIRS^{initial} demonstrating the advantages attained with the use of new vicarious calibration gains. Furthermore, with the VIIRS$^{12.2}$, spectral shape consistency between the satellite and in-situ SeaPRISM $nLw(\lambda)$ data is not only enhanced but biases between the two data at every wavelengths are also reduced. Nevertheless, slight underestimations with spectral average *PD* value equal to ~6% still exist in VIIRS$^{12.2}$. Conversely, for LISCO site, it is observed that the VIIRS^{initial} achieves the stronger overall correlation with *R* value equal to 0.961 compared to 0.919 with the VIIRS$^{12.2}$. In addition, VIIRS$^{12.2}$ data for LISCO site shows more frequent occurrences of the negative normalized water-leaving radiances especially at 413 nm, and underestimation is further exacerbated to −26% on spectral average. These observations point out that the impacts of the version 2012.2 processing scheme on sensor radiance data in retrieving *nLw* data is not the same for each site. These considerations probably suggest the need to take into account comparisons between AERONET-OC and satellite data for coastal sites before making decisions on changes of sensor gains.

Strong consistency between the time-series *nLw* data retrieved from the VIIRS and MODIS sensors was also observed particularly through the large *R* values (0.838–0.994) obtained for the comparisons at every wavelength. Nevertheless, uncertainties between the *nLw* data retrieved by the two sensors are high at 413 nm with both VIIRS processing. At that wavelength, *APD* values obtained for the VIIRS versus MODIS *nLw* match-up comparisons are in the order of 50% exhibiting the need for the refinement in the calibration and processing procedures. On the other hand, for the wavelengths greater 442 nm, uncertainties between the MODIS and VIIRS data are relatively low with their *APD* values observed to be around 10% and uncertainties are lowest at 551 nm with *APD* value equal to 3.9%.

Initial assessments of the IDPS output of the VIIRS shows that, with the processing, normalized water-leaving radiance at 551 nm are overestimated, and for all other wavelengths they are underestimated. For the WaveCIS site, strong correlation between the VIIRS^{IDPS} and in-situ SeaPRISM data is observed at every wavelength. For the LISCO site, although very few spectra are available, they show excellent agreement with the SeaPRISM data. Correlations between satellite and AERONET-OC data were found to be similar for WaveCIS site when NASA or IDPS processing schemes were used.

Investigations on the aerosol model selection suggest that spectral behavior of the aerosol optical properties cannot be fully apprehended resulting in underestimated VIIRS retrieved Angstrom exponent values. Nevertheless, for both LISCO and WaveCIS sites, in-situ and VIIRS retrieved τ_a values are significantly correlated with values of the coefficient of correlation *R* equal to 0.959 and 0.951 at 443 nm and 870 nm wavelengths respectively for WaveCIS site, and 0.894 and 0.903 for LISCO site. On the other hand, overestimations in VIIRS retrieved τ_a values are observed for both sites at both 442 and 870 nm wavelengths. Nevertheless, overestimations in MODIS retrieved τ_a values are much less than those observed for VIIRS. It may be helpful to revisit the atmospheric correction algorithm to improve the fine mode aerosol determination. Another way to follow would be to design novel calibration procedure for the VIIRS *NIR* 862 nm band.

Acknowledgments

This work was partially supported by grants from the Office of Naval Research and National Oceanic and Atmospheric Administration. We would like to thank the NASA AERONET team for SeaPRISM calibration, data processing, and support of site operations and the NASA Ocean Color Processing Group and NOAA for satellite imagery. We are also grateful to two anonymous reviewers for their helpful suggestions. The views, opinions, and findings contained in this paper are those of the authors and should not be construed as an official NOAA or U.S. Government position, policy, or decision.

References

Ahmad, Z., Franz, B.A., McClain, C. R., Kwiatkowska, E. J., Werdell, J., Shettle, E. P., et al. (2010). New aerosol models for the retrieval of aerosol optical thickness and normalized water-leaving radiances from the SeaWiFS and MODIS sensors over coastal regions and open oceans. *Applied Optics, 49*, 5545–5560.

Ahmed, S., Gilerson, A., Harmel, T., Hlaing, S., Tonizzo, A., Weidemann, A., et al. (2012). Evaluation of atmospheric correction procedures for ocean color data processing using hyper-and multi-spectral radiometric measurements from the Long Island Sound Coastal Observatory. *Proc. of SPIE Vol* (pp. 83720M–83721M).

Bailey, S. W., Franz, B.A., & Werdell, P. J. (2010). Estimation of near-infrared water-leaving reflectance for satellite ocean color data processing. *Optics Express, 18*, 7521–7527.

Bricaud, A., Morel, A., Babin, M., Allali, K., & Claustre, H. (1998). Variations of light absorption by suspended particles with chlorophyll a concentration in oceanic (case 1) waters: Analysis and implications for bio-optical models. *Journal of Geophysical Research, 103*, 31033–31044.

Bulgarelli, B., & Zibordi, G. (2003). Remote sensing of ocean colour: Accuracy assessment of an approximate atmospheric correction method. *International Journal of Remote Sensing, 24*, 491–509.

Clark, D., Gordon, H., Voss, K., Ge, Y., Broenkow, W., & Trees, C. (1997). Validation of atmospheric correction over the oceans. *Journal of Geophysical Research, 102*, 209–217.

Clark, D. K., Yarbrough, M.A., Feinholz, M., Flora, S., Broenkow, W., Kim, Y. S., et al. (2003). MOBY, a radiometric buoy for performance monitoring and vicarious calibration of

satellite ocean color sensors: Measurement and data analysis protocols. *Ocean Optics Protocols for Satellite Ocean Color Sensor Validation, Revision, 4*, 3–34.

Committee on Assessing Requirements for Sustained Ocean Color Research (2011). *Assessing the requirements for sustained ocean color research and operations.* : National Academies Press.

Cox, C., & Munk, W. (1954). Statistics of the sea surface derived from sun glitter. *Journal of Marine Research, 13*, 198–227.

Deschamps, P. Y., Herman, M., & Tanre, D. (1983). Modeling of the atmospheric effects and its application to the remote sensing of ocean color. *Applied Optics, 22*, 3751–3758.

Franz, B.A., Bailey, S. W., Werdell, P. J., & McClain, C. R. (2007). Sensor-independent approach to the vicarious calibration of satellite ocean color radiometry. *Applied Optics, 46*, 5068–5082.

Frouin, R., Schwindling, M., & Deschamps, P. Y. (1996). Spectral reflectance of sea foam in the visible and near-infrared: In situ measurements and remote sensing implications. *Journal of Geophysical Research, 101* (14361-14314,14371).

Gordon, H. R. (1998). In-orbit calibration strategy for ocean color sensors. *Remote Sensing of Environment, 63*, 265–278.

Gordon, H. R. (2005). Normalized water-leaving radiance: Revisiting the influence of surface roughness. *Applied Optics, 44*, 241–248.

Gordon, H. R., Du, T., & Zhang, T. (1997). Remote sensing of ocean color and aerosol properties: Resolving the issue of aerosol absorption. *Applied Optics, 36*, 8670–8684.

Gordon, H. R., & Wang, M. (1992). Surface roughness considerations for atmospheric correction of ocean color sensors. 1: The Rayleigh scattering component. *Applied Optics, 31*, 4247–4260.

Gordon, H. R., & Wang, M. (1994a). Retrieval of water leaving radiance and aerosol optical thickness over the oceans with SeaWiFS: A preliminary algorithm. *Applied Optics, 33*, 443–458.

Gordon, H. R., & Wang, M. (1994b). Influence of oceanic whitecaps on atmospheric correction of ocean-color sensors. *Applied Optics, 33*, 7754–7763.

Hansen, J. E., & Travis, L. D. (1974). Light scattering in planetary atmospheres. *Space Science Reviews, 16*, 527.

Harmel, T., Gilerson, A., Hlaing, S., Tonizzo, A., Legbandt, T., Weidemann, A., et al. (2011). Long Island Sound Coastal Observatory: Assessment of above-water radiometric measurement uncertainties using collocated multi and hyperspectral systems. *Applied Optics, 50*, 5842–5860.

Hlaing, S., Gilerson, A., Harmel, T., Tonizzo, A., Weidemann, A., Arnone, R., et al. (2012). Assessment of a bidirectional reflectance distribution correction of above-water and satellite water-leaving radiance in coastal waters. *Applied Optics, 51*, 220–237.

Hooker, S. B., Zibordi, G., Berthon, J. F., & Brown, J. W. (2004). Above-water radiometry in shallow coastal waters. *Applied Optics, 43*, 4254–4268.

Hu, C., Carder, K. L., & Muller-Karger, F. E. (2000). Atmospheric correction of SeaWiFS imagery over turbid coastal waters: A practical method. *Remote Sensing of Environment, 74*, 195–206.

IOCCG (2008). Why ocean colour? The societal benefits of ocean-colour technology. In T. Platt, N. Hoepffner, V. Stuart, & C. Brown (Eds.), *Reports of the International Ocean-Colour Coordinating Group, No. 7*, Dartmouth, Canada: IOCCG.

IOCCG (2010). Atmospheric correction for remotely-sensed ocean-colour products. In M. Wang (Ed.), *Reports of International Ocean-Color Coordinating Group, No. 10*, Dartmouth, Canada: IOCCG.

Lee, Z., Carder, K. L., & Arnone, R. A. (2002). Deriving inherent optical properties from water color: A multiband quasi-analytical algorithm for optically deep waters. *Applied Optics, 41*, 5755–5772.

Meister, G., Franz, B.A., Kwiatkowska, E. J., & McClain, C. R. (2012). Corrections to the calibration of MODIS Aqua ocean color bands derived from SeaWiFS data. *IEEE Transactions on Geoscience and Remote Sensing, 50*, 310–319.

Morel, A., Antoine, D., & Gentili, B. (2002). Bidirectional reflectance of oceanic waters: Accounting for Raman emission and varying particle scattering phase function. *Applied Optics, 41*, 6289–6306.

Murphy, R. E., Barnes, W. L., Lyapustin, A. I., Privette, J., Welsch, C., DeLuccia, F., et al. (2001). Using VIIRS to provide data continuity with MODIS. *Geoscience and Remote Sensing Symposium, 2001. IGARSS'01. IEEE 2001 International* (pp. 1212–1214).

Ruddick, K. G., Ovidio, F., & Rijkeboer, M. (2000). Atmospheric correction of SeaWiFS imagery for turbid coastal and inland waters. *Applied Optics, 39*, 897–912.

Shettle, E. P., & Fenn, R. W. (1979). *Models for the aerosols of the lower atmosphere and the effects of humidity variations on their optical properties.* Hanscomb Air Force Base, MA: U.S. Air Force Geophysics Laboratory 01731,AFGL-TR-79-02 14.

Siegel, D. A., Wang, M., Maritorena, S., & Robinson, W. (2000). Atmospheric correction of satellite ocean color imagery: The black pixel assumption. *Applied Optics, 39*, 3582–3591.

Stumpf, R. P., Arnone, R. A., Gould, R. W., Martinolich, P.M., & Ransibrahmanakul, V. (2003). A partially coupled ocean–atmosphere model for retrieval of water-leaving radiance from SeaWiFS in coastal waters. *NASA Technical Memorandum, 206892*, 51–59.

Sydor, M., & Arnone, R. A. (1997). Effect of suspended particulate and dissolved organic matter on remote sensing of coastal and riverine waters. *Applied Optics, 36*, 6905–6912.

Tanre, D., Herman, M., Deschamps, P. Y., & Deleffe, A. (1979). Atmospheric modeling for space measurements of ground reflectances, including bidirectional properties. *Applied Optics, 18*, 3587–3594.

Thuillier, G., Herse, M., Labs, D., Foujols, T., Peetermans, W., Gillotay, D., et al. (2003). The solar spectral irradiance from 200 to 2400 nm as measured by the SOLSPEC spectrometer from the ATLAS and EURECA missions. *Solar Physics, 214*, 1–22.

Voss, K. J., & Morel, A. (2005). Bidirectional reflectance function for oceanic waters with varying chlorophyll concentrations: Measurements versus predictions. *Limnology and Oceanography, 698–705*.

Wang, M. (2002). The Rayleigh lookup tables for the SeaWiFS data processing: Accounting for the effects of ocean surface roughness. *International Journal of Remote Sensing, 23*, 2693–2702.

Wang, M. (2005). A refinement for the Rayleigh radiance computation with variation of the atmospheric pressure. *International Journal of Remote Sensing, 26*, 5651–5663.

Wang, M. (2006). Effects of ocean surface reflectance variation with solar elevation on normalized water-leaving radiance. *Applied Optics, 45*, 4122–4128.

Wang, M. (2007). Remote sensing of the ocean contributions from ultraviolet to near-infrared using the shortwave infrared bands: Simulations. *Applied Optics, 46*, 1535–1547.

Wang, M., & Bailey, S. W. (2001). Correction of sun glint contamination on the SeaWiFS ocean and atmosphere products. *Applied Optics, 40*, 4790–4798.

Wang, M., & Gordon, H. R. (2002). Calibration of ocean color scanners: How much error is acceptable in the near infrared? *Remote Sensing of Environment, 82*, 497–504.

Wang, M., Knobelspiesse, K. D., & McClain, C. R. (2005). Study of the Sea-Viewing Wide Field-of-View Sensor (SeaWiFS) aerosol optical property data over ocean in combination with the ocean color products. *Journal of Geophysical Research, 110*, D10S06.

Wang, M., & Shi, W. (2005). Estimation of ocean contribution at the MODIS near-infrared wavelengths along the east coast of the US: Two case studies. *Geophysical Research Letters, 32*, L13606.

Wang, M. H., & Shi, W. (2007). The NIR–SWIR combined atmospheric correction approach for MODIS ocean color data processing. *Optics Express, 15*, 15722–15733.

Werdell, P. J., Bailey, S. W., Franz, B.A., Morel, A., & McClain, C. R. (2007). On-orbit vicarious calibration of ocean color sensors using an ocean surface reflectance model. *Applied Optics, 46*, 5649–5666.

Zibordi, G., Berthon, J. F., Mélin, F., D'Alimonte, D., & Kaitala, S. (2009). Validation of satellite ocean color primary products at optically complex coastal sites: Northern Adriatic Sea, Northern Baltic Proper and Gulf of Finland. *Remote Sensing of Environment, 113*, 2574–2591.

Zibordi, G., Mélin, F., Berthon, J. F., Holben, B., Slutsker, I., Giles, D., et al. (2009). AERONET-OC: A network for the validation of ocean color primary products. *Journal of Atmospheric and Oceanic Technology, 26*, 1634–1651.

Zibordi, G., Mélin, F., Hooker, S. B., D'Alimonte, D., & Holben, B. (2004). An autonomous above-water system for the validation of ocean color radiance data. *IEEE Transactions on Geoscience and Remote Sensing, 42*, 401–415.